

COMPARISON OF A MODIFIED HYBRID III ATD TO A HUMAN TEST PILOT DURING  
POWER WHEELCHAIR DRIVING

by

Michael Joseph Dvorznak

BS; Mechanical Engineering, Carnegie Mellon University, 1997

Submitted to the Graduate Faculty of  
The School of Engineering in partial fulfillment  
of the requirements for the degree of  
Master of Science in Bioengineering

University of Pittsburgh

2003

UNIVERSITY OF PITTSBURGH

SCHOOL OF ENGINEERING

This thesis was presented

by

Michael Joseph Dvorznak

It was defended on

September 25, 2002

and approved by

Michael L. Boninger, Adjunct Professor, Bioengineering

Songfeng Guo, Associate Professor, Bioengineering

Thesis Advisor: Rory A. Cooper, Professor, Bioengineering

## ABSTRACT

### COMPARISON OF A MODIFIED HYBRID III ATD TO A HUMAN TEST PILOT DURING POWER WHEELCHAIR DRIVING

Michael Dvorznak, MS

University of Pittsburgh, 2003

It is estimated that there are 85,000 serious wheelchair accidents annually, of which 80% are attributable to tips and falls. Despite the increasing trend in wheelchair accidents every year, there is little literature on the cause and prevention of these accidents. Test dummies provide an ethical and practical alternative to subjects when assessing the risks and prevention mechanisms of tips and falls in controlled studies. However, design criteria for anthropomorphic test devices (ATDs) were based on the response and tolerance data acquired from cadaver studies and human volunteers. Such cadavers are typically of advanced age, and have anthropometrics reflecting a healthy, unimpaired population. For that reason, use of ATDs in relatively low speed wheelchair studies may under estimate the risk of injury.

The purpose of this study was to develop and validate a low speed, low impact test dummy for use in the study of the prevention of tips and falls from wheelchairs. A kinematic analysis comparing the trunk bending of a Hybrid III test dummy (HTD) to that of a wheelchair user during various braking trials served for validation. In addition, a dynamic model was used to determine underlying causes of the motion.

Statistical differences were not found ( $p > .05$ ) in the peak trunk angular range of motion, velocity, and acceleration measures of a modified HTD over a range of wheelchair speeds and decelerations. This is promising evidence that the test dummy is a suitable surrogate for a

wheelchair user in low speed dynamic studies. However, the HTD underestimated the motion of a wheelchair test pilot during the fast speed and power-off braking condition.

A dynamic model consisting of a cart with an inverted pendulum was used to provide additional insight into the differences in motion. Although the model produced consistent values for damping and stiffness coefficients, evidence indicates that the functional form of the model may be incorrect. The model likely estimated properties for a wheelchair/rider system rather than only the rider. Further analysis showed an impingement occurring between the pelvis and thighs of the HTD. Removing the impingement will further increase the similarities between the HTD and test pilot.

## ACKNOWLEDGMENTS

I would like to thank my advisor, Dr. Cooper, for providing the opportunity and the environment to learn and conduct this research. I would also like to express my appreciation to Dr. Guo and Dr. Boninger for their time and patience while serving as members of the thesis committee and their insightful comments. I would also like to thank all of the students at HERL who aided with data collection for this study.

I extend my deepest gratitude to my mother and father for their love, support, and encouragement throughout my educational endeavors and my sister, Michele, who put the pressure on and made it a race to see who could finish first their degree first (she won). I could not have accomplished this without you.

## TABLE OF CONTENTS

1.0 INTRODUCTION .....	1
2.0 METHODS .....	4
2.1 Test Cases .....	4
2.2 Test Wheelchair .....	8
2.3 Measurement System .....	8
2.4 Validation Concept .....	9
2.5 Experimental Protocol .....	10
2.6 Data Reduction.....	13
2.6.1 Kinematic Comparison .....	13
2.6.2 Dynamic Model .....	15
3.0 RESULTS .....	18
4.0 DISCUSSION .....	22
4.1 Kinematic Comparison .....	22
4.2 Dynamic Model .....	24
APPENDIX A.....	32
DERIVATION OF EQUATIONS OF MOTION FOR CART WITH AN INVERTED PENDULUM SYSTEM.....	32
APPENDIX B .....	35
GRAPHICAL RESIDUAL ANALYSIS .....	35
APPENDIX C .....	39
COMPOSITION OF FORCING VARIABLE .....	39

APPENDIX D.....	40
MATLAB PROGRAMS.....	40
BIBLIOGRAPHY.....	58

## LIST OF TABLES

Table 1 Test case characteristics.....	7
Table 2 The means $\pm$ (SD) of the wheelchair speed at brake initiation, trunk angular displacement (TAD), velocity (TAV), and acceleration (TAA) are compared between the Hybrid III (HTD) and test pilot (TP) for the three braking conditions, joystick release (JR), joystick full reverse (FR), and emergency power off (EPO). No statistical differences were present between the TP and HTD for all measures.....	18
Table 3 Model parameters of the test pilot and HTD. ....	21
Table 4 “Loss of controls” experienced by test cases during braking trials. ....	23

## LIST OF FIGURES

Figure 1 CNC milled custom pelvic base. ....	5
Figure 2 CNC milled load cell adapter plate. ....	5
Figure 3 HTD pelvis showing straight lumbar spine, pelvic base, and load cell adapter plate. ....	6
Figure 4 Pedestrian pelvis with trimmed thighs, buttocks removed and foam inserts around hips to mimic flaccid tissue. ....	7
Figure 5 Seated position of the test pilot and test equipment. ....	9
Figure 6 Determination of joystick release brake initiation.....	11
Figure 7 Determination of joystick full reverse brake initiation.....	11
Figure 8 Determination of emergency power off brake initiation. ....	12
Figure 9 Hybrid III test dummy showing following marker locations: 1) ear, 2) shoulder, 3) hip, 4) knee, 5) corner of frame (intersection of seat pan and backrest) 6) front edge of seat 7) bottom of joystick stem 8) top of joystick stem.....	14
Figure 10 Inverted pendulum model and free body diagrams. ....	15
Figure 11 Trunk angular displacement of the test pilot and HTD during 2m/s, emergency power off braking.....	19
Figure 12 Trunk angular velocity of the test pilot and HTD during 2m/s, emergency power off braking. ....	19
Figure 13 Trunk angular acceleration of the test pilot and HTD during 2m/s, emergency power off braking.....	20
Figure 14 Center of gravity angular displacement for one trial of the test pilot and HTD during the middle speed, emergency power off braking. ....	27
Figure 15 Center of gravity angular displacement of the test pilot and HTD near the end of the 2 m/s emergency power off braking trials. ....	29

Figure 16 Free body diagrams of cart with an inverted pendulum system. .... 32

Figure 17 Residual from all trials involving test pilot vs. the model parameter, center of gravity angle. .... 35

Figure 18 Residual from all trials involving test pilot vs. the center of gravity angular velocity. 36

Figure 19 Residual from all trials involving HTD vs. the model parameter, center of gravity angle. .... 37

Figure 20 Residual from all trials involving HTD vs. the center of gravity angular velocity. .... 38

Figure 21 Composition of forcing variable. .... 39

## 1.0 INTRODUCTION

Most power wheelchair users have impairments to both lower and upper extremities. These impairments may make it difficult to maintain the body in an upright-seated posture, especially when the upper body is subjected to forces [1]. A study by Kirby et al. estimated that there are about 85,000 serious wheelchair accidents annually with a significant upward trend over time [2]. This represents about 4.3% of the wheelchair user population. Between 1973 and 1987, 770 wheelchair related deaths were reported to the United States Consumer Product Safety Commission (USCPSC), 77.4% of which were attributed to falls and tips [3]. Of the 2,066 nonfatal accidents reported between 1986 and 1990 to the USCPSC, falls and tips were the cause 73.2% of the time [4]. It is important that the incidence and severity of these accidents are reduced and wheelchairs are made safer. To accomplish this, the cause of the falls must be investigated.

Wheelchair testing with living human subjects would provide the best human response measures and, thus, the most insight into accident prevention. Due to the nature of the observed problem, it is not always practical or ethical to use a person in a wheelchair to assess the risks and prevention mechanisms of tips and falls. Any experimental impact of human volunteers must be conducted below pain and injury thresholds. In addition, people cannot be easily instrumented with measurement devices [5].

The unembalmed cadaver is possibly the best surrogate. It has the advantage of possessing the identical anthropometrics and organ distribution of a living human and sustains almost all of the injuries seen in accident victims [6&7]. Human cadavers are not easily available; though, and do not provide repeatable data [5]. Therefore, the evaluation of safety systems in which repeated measurements may be done, should be performed using human-like

test dummies [6]. The Hybrid series of test dummies developed by General Motors are industry standards in vehicle crash testing. These test dummies have been proven to be very repeatable, reproducible, durable, and serviceable test devices [8]. Whereas test dummies have limited applicability for describing actual injuries, they may provide insight into the injury mechanisms through impact response and tolerance data. Rather than actually “injuring” the test dummy, levels of biomechanical response are established that are deemed likely to result in injury if the test dummy was human [6]. These response/injury thresholds are called injury criteria and different criteria are used for different regions of the body [9].

The use of anthropomorphic test dummies (ATDs) to study wheelchair stability and driving accidents is not a new concept. Kirby used a Hybrid II test dummy to study the effects of locking the brakes in rearward tipping accidents [10]. Sosner utilized a 50<sup>th</sup> percentile Hybrid III dummy and depot-type wheelchair to simulate three types of curb negotiation accidents [11]. Fast employed a Hybrid III in studying the effect of restraining systems (lap belt and four-point restraint) on curb negotiation accidents [12]. Cooper used a 50<sup>th</sup> percentile Hybrid II to examine the safety of 8 power wheelchairs during braking [1]. The design criteria for ATDs were based on the response and tolerance data acquired from cadaver studies. Such cadavers are typically of advanced age, and have anthropometrics reflecting a healthy, unimpaired population. In addition, vehicle crash testing occurs at higher speeds and accelerations at which lack of muscular activity can be ignored due to reaction time [5]. For these reasons, use of ATDs in relatively low-speed wheelchair studies may underestimate the risk of injury.

The purpose of this study was to develop and validate a low speed, low impact test dummy for use in the study of the prevention of tips and falls from wheelchairs. A kinematic analysis comparing the trunk bending of a Hybrid III test dummy to that of a wheelchair user during various braking trials was implemented for validation. In addition, a dynamic model was used to determine underlying causes of the motion.

## 2.0 METHODS

### 2.1 Test Cases

A 50<sup>th</sup> percentile male Hybrid III anthropomorphic test dummy (HTD) was used to simulate the occupant of a power wheelchair. The HTD series comes equipped standard with a seated pelvis and curved lumbar spine so the HTD can assume an “automotive seated position” [13]. When investigating the nature of power wheelchair accidents, the occupant may not necessarily remain in a seated posture in the occurrence of a fall. To accommodate for this, a standing “pedestrian” pelvis with the accompanying straight lumbar spine was utilized in place of the seated pelvis with curved lumbar spine. In addition to being the complementary component for the standing pelvis, the straight lumbar spine has a lower stiffness in flexion and extension than the curved lumbar spine (48 versus 203 in-lbf/deg) [14]. For purposes of clarity, the rotational units will be omitted and angular units of radians will be assumed. For instance, the units of the coefficient of damping will be reported in Nms rather than Nms/rad. The custom pelvic base seen in Figure 1 and load cell adapter plate, Figure 2, were fabricated on a CNC milling machine to enable the existing standard instrumentation to be used with the design changes.

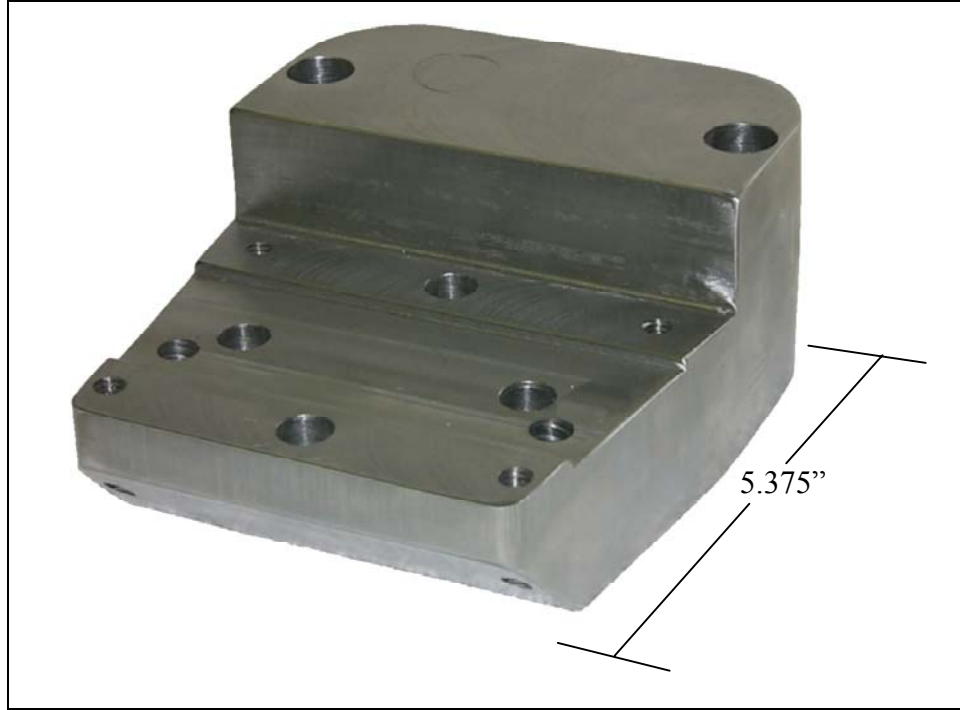


**Figure 1 CNC milled custom pelvic base.**

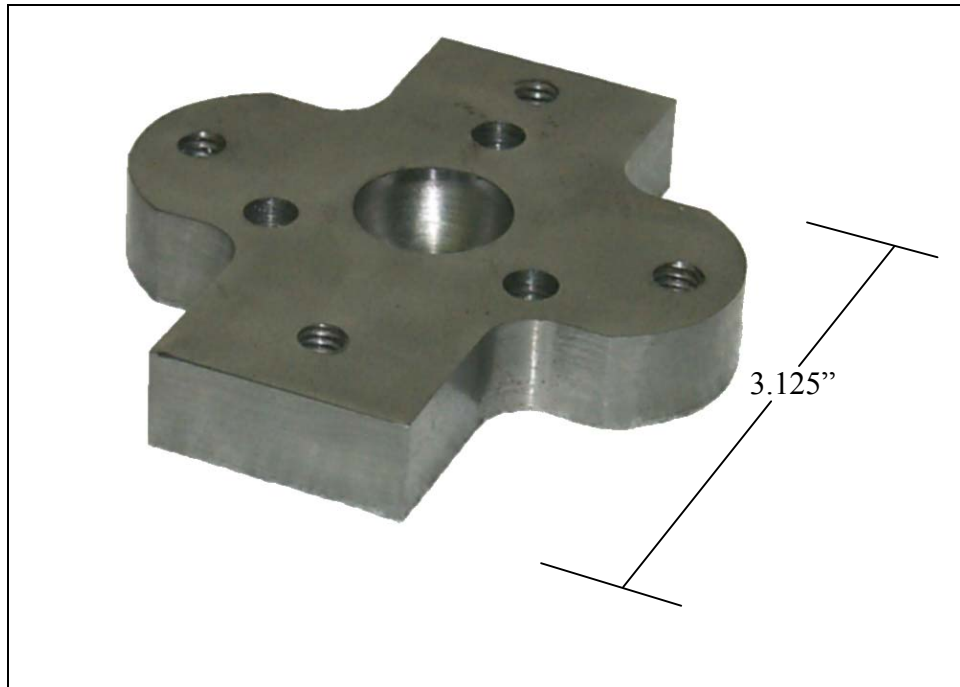


**Figure 2 CNC milled load cell adapter plate.**

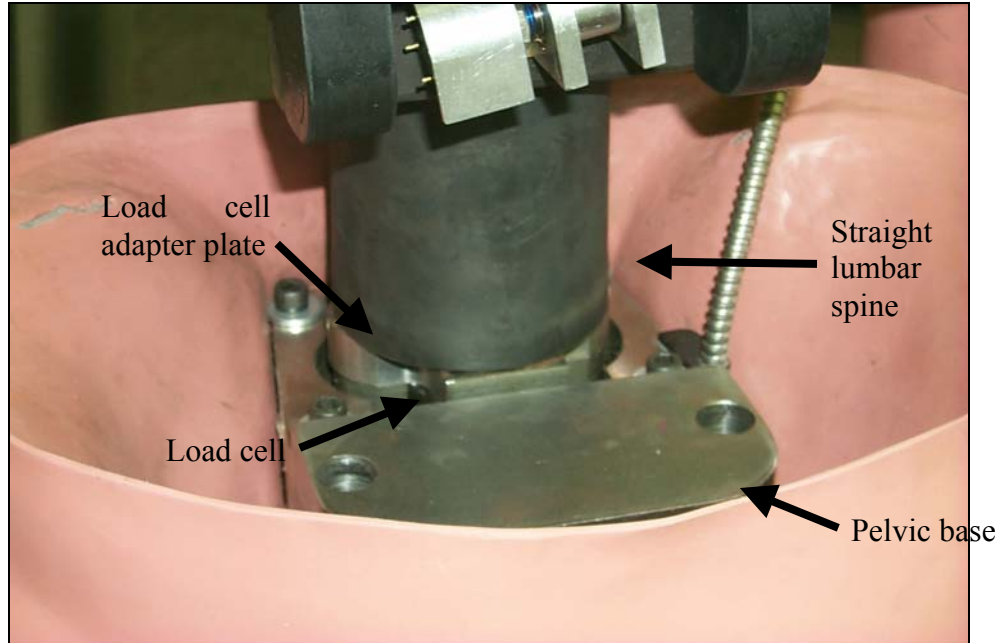


**Figure 3 HTD pelvis showing straight lumbar spine, pelvic base, and load cell adapter plate.**

Vinyl coated foam “tissue” was removed from the inner thighs of the HTD to allow for a non-interference fit during seated posture. Further modifications were made based on the hypothesis that bending in a forward fall from a wheelchair occurs mostly from flexion in the hip joints, with additional contribution from flexion in the lumbar region of the spine. The foam/rubber buttocks were removed and instead low-density polyurethane foam was used to mimic flaccid tissue [15, 16] (Figure 4). This allowed more freedom in the test dummy’s hip joint. The abdomen was removed to reduce trunk resistance. This was shown to provide more realistic motion in a Hybrid II test dummy [17].



**Figure 4 Pedestrian pelvis with trimmed thighs, buttocks removed and foam inserts around hips to mimic flaccid tissue.**

A single wheelchair user with T8 paraplegia due to traumatic spinal cord injury was used for comparison. Table 1 details the demographics and anthropometrics of the test cases.

**Table 1 Test case characteristics.**

Test case	Sex	Age	Mass (kg)	Height (mm)	Diagnosis
Test Pilot	Male	42	55	177	T8 SCI
HTD	Male	NA	75	171	Modified

Markers were placed on the knee, hip, shoulder, and front of the ear of both test cases to describe the motion of the trunk. In addition, markers were placed on the elbow and wrist of the test pilot for the calculation of the upper body center of gravity and mass moment of inertia. This was not necessary with the HTD because the bolts in the arm and shoulder were tightened so that no motion of the arms could occur relative to the upper body.

## 2.2 Test Wheelchair

Testing was performed using one power wheelchair as the input: a Quickie P100 (Sunrise Medical, Inc.). The P100 was selected based upon availability at our research center and because it presented minimal risk of causing a fall to the test pilot as determined in a previous study [1]. Both the HTD and test pilot were seated on a 50mm polyurethane foam cushion. Markers were placed on the front edge of the seat pan and at the intersection of the seat pan and back support for determining wheelchair velocity, acceleration, and orientation and on the stem of the joystick to obtain joystick position.

## 2.3 Measurement System

An OPTOTRAK 3020 (Northern Digital, Inc., Waterloo, Canada) motion measurement system was used to collect 3D position data. The system utilizes active infrared emitting diode (IRED) markers to alleviate problems of marker confusion and relocation. The system has a resolution of .01 mm at a distance of 2.25 m and rms accuracy of .1 mm in the x,y (width, height) directions and .15 mm in the z direction (depth) [18]. The position sensor with a “far focus” was located 5.5 m from the line of action of the wheelchair in order to contain the motion within the field of view. Raw data were sampled at 240 Hz with a marker frequency of 2500 Hz. Raw data were converted to 3D marker position data that were filtered before analyses. HTD and test pilot marker data were conditioned using a 4<sup>th</sup> order, zero lag, low-pass Butterworth filter at a 6 Hz cutoff frequency [19]. Wheelchair data were filtered similarly but with a 12 Hz cutoff frequency because power spectral density estimates indicated signal power at higher frequencies.

## 2.4 Validation Concept

The test dummy was clothed to provide similar friction with the seat as the test pilot. A kinematic analysis of the trunk bending during a braking trial was used to endorse the modifications to the HTD. Active markers were fixed to the shoulder, hip, and knee to capture the trunk motion. The HTD and test pilot were seated in the wheelchair as depicted in Figure 5 with arms abducted and forearms flexed to prevent using them for support during trials. While the test pilot was seated in the chair, two spotters were positioned approximately 1.5 meters beyond the braking line to intervene in case of falls.



**Figure 5 Seated position of the test pilot and test equipment.**

## 2.5 Experimental Protocol

Testing was performed at the Human Engineering Research Laboratories. Test protocol included three braking conditions: joystick release, joystick full reverse, and emergency power-off. In addition, the braking conditions were enacted with three power wheelchair initial velocities: slow (0.8m/s), medium (1.4m/s), and fast (2.0m/s). The slowest speed was obtained by turning the potentiometer on the joystick to its minimum value. Likewise, the maximum speed was achieved by turning the potentiometer to its maximum value. The potentiometer was tuned to provide a mid-range speed. One test operator drove the P100 from the right side without obscuring the markers. A 6-meter run-up area was used to achieve the selected speed of the wheelchair. The test operator initiated the braking scenario when the front caster crossed a braking line labeled on the floor. Position data from the joystick, as well as velocity and acceleration curves of the wheelchair were analyzed to determine the start of braking. Figure 6 illustrates how the joystick angle was used to determine the data index at which joystick release braking was initiated. When in the neutral position, the joystick is at approximately 90° to the horizontal. When the right caster crossed a braking line on the floor, the joystick was released by slipping the thumb off of the top of the joystick stem. This method produces the small increase in angle seen just prior to the rapid decrease in joystick angle. The beginning of the joystick release was the frame that the maximum angle occurred, noted in the figure with a red “x”. Figure 7 illustrates how the joystick angle was used to determine the data index at which full reverse braking was initiated. Full reverse braking was considered to begin when the joystick passed the neutral position (approximately 90°). To minimize error, the index corresponding to the joystick angle closest to 90° was considered as the start of braking.

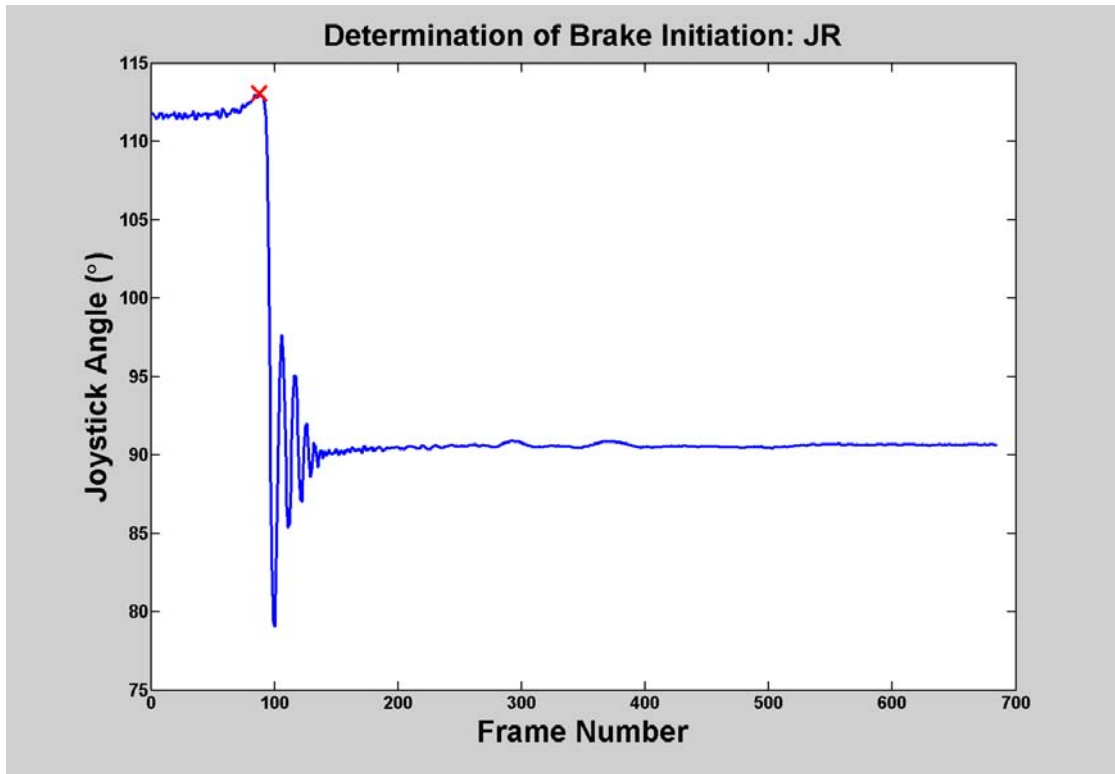


Figure 6 Determination of joystick release brake initiation.

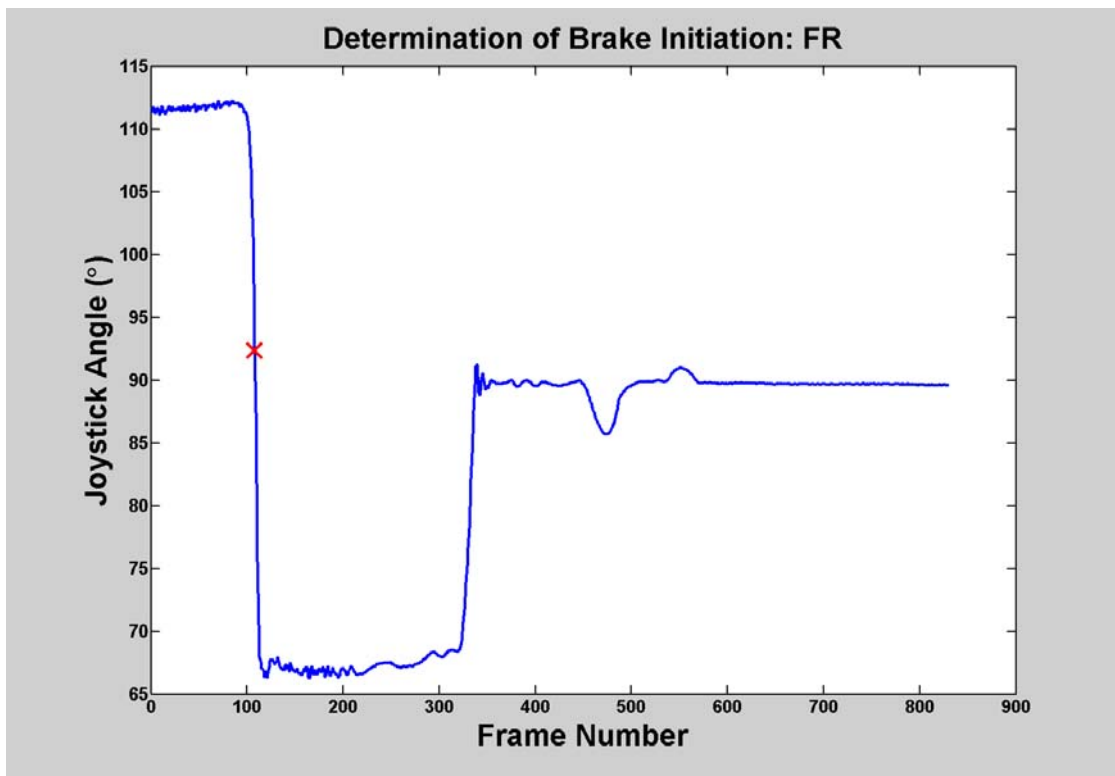
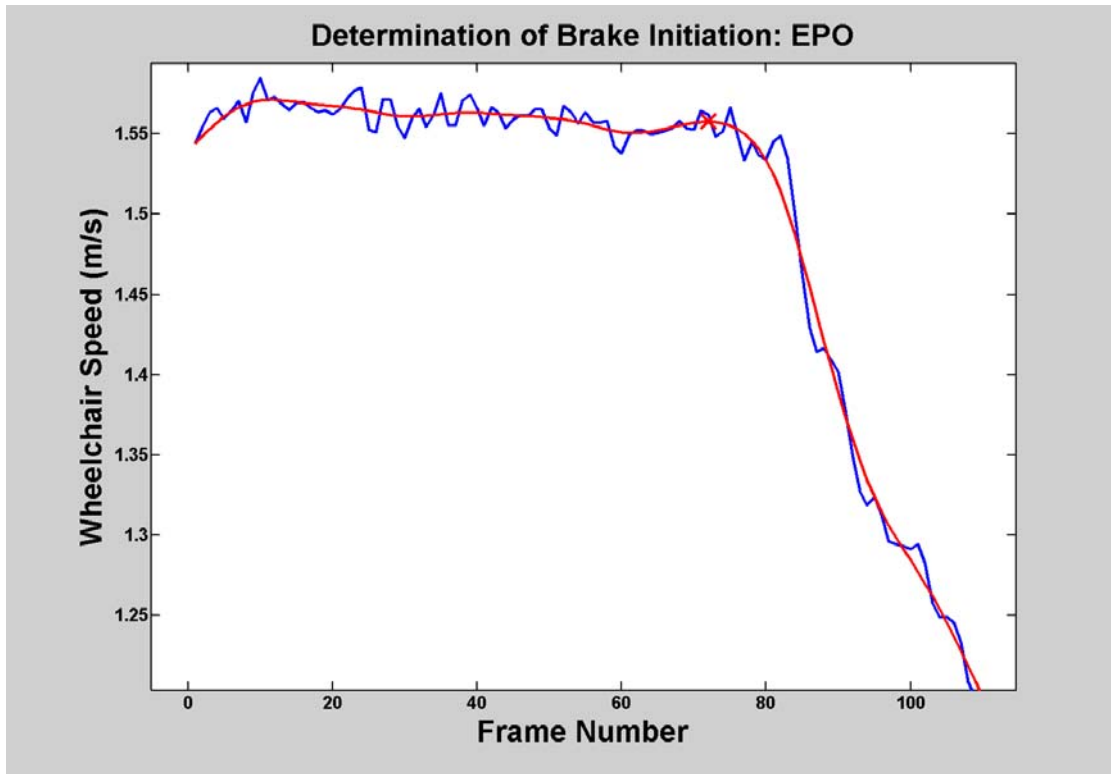


Figure 7 Determination of joystick full reverse brake initiation.



**Figure 8** Determination of emergency power off brake initiation.

Figure 8 illustrates the use of the wheelchair speed in determining the data index at which emergency power off braking was initiated. The blue line is the unfiltered velocity of the wheelchair and the red line is the wheelchair speed after filtering with a 4th order, zero lag, low-pass Butterworth filter at a 12 Hz cutoff frequency. The start of EPO braking is defined as the maximum velocity (or zero acceleration) immediately preceding the rapid deceleration. This point is marked with a red “x” above.

## 2.6 Data Reduction

### 2.6.1 Kinematic Comparison

The trunk angle was measured by computing the angle between the knee, hip, and shoulder markers (markers 4, 3, and 2 in Figure 9) in the sagittal plane. The angle was determined in reference to the angle of the trunk when braking was initiated. This results in the range of motion of the trunk during the braking scenario.

Successive time derivatives of the trunk angular displacement were calculated numerically to obtain trunk angular velocity, and acceleration. The trunk kinematics were used as measures of comparison between the test pilot and HTD. For statistical purposes, the maximum value on each of the curves was indicated. The average peak angular displacement, velocity, and acceleration were calculated from four trials. Paired T-tests were used to detect differences between the test dummy and test pilot. Pairs were associated by speed and braking condition, yielding nine pairs. A significance level of  $\alpha=.05$  was set *a priori*.



**Figure 9 Hybrid III test dummy showing following marker locations: 1) ear, 2) shoulder, 3) hip, 4) knee, 5) corner of frame (intersection of seat pan and backrest) 6) front edge of seat 7) bottom of joystick stem 8) top of joystick stem.**

Analysis of the peak trunk kinematic values provides a simple and convenient method to detect differences. However, this analysis omits valuable time-series information about the shape of the curves. In addition, if differences are present, the maximum values provide little insight into the underlying causes of those differences.

## 2.6.2 Dynamic Model

A model based on the physical laws of nature was developed to characterize the motion. A classical cart with an inverted pendulum, studied commonly in control systems theory, was modeled for the wheelchair/rider system. The hip joint plays the role of the fulcrum of the inverted pendulum. The masses of the pelvis, trunk, head, and arms comprise the mass of the pendulum. The pendulum was considered to have inertia,  $J$ , about the fulcrum, a viscous damping constant,  $B$ , and stiffness,  $K$ . Inputs to the system are provided by the acceleration of the power wheelchair and gravity effects. Two free body diagrams (FBD) of the system are pictured in Figure 10.

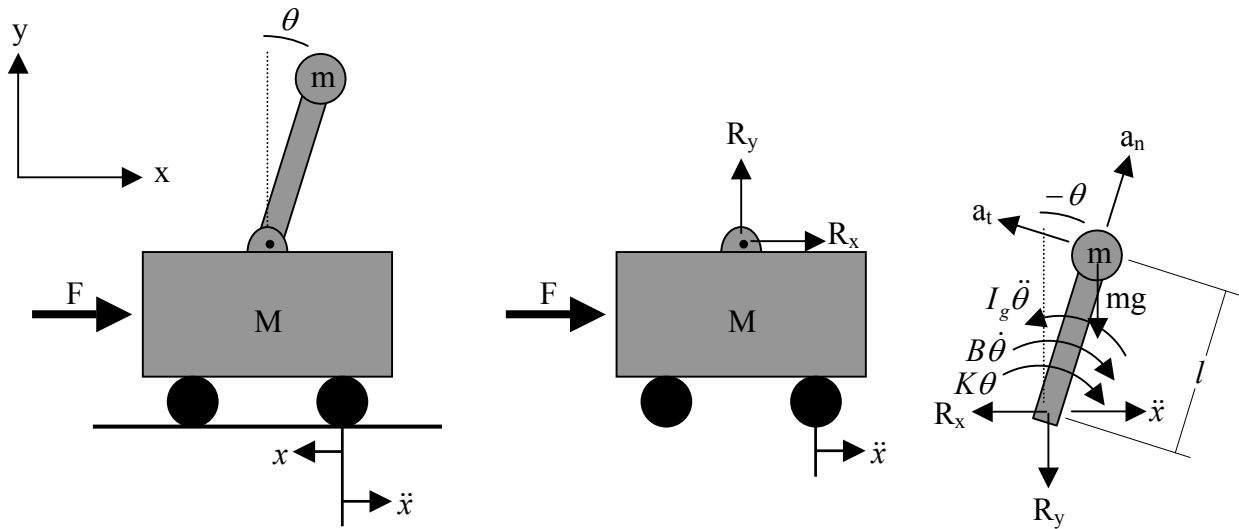


**Figure 10** Inverted pendulum model and free body diagrams.

Applying D'Alembert's principal leads to this form of the dynamic equation for the inverted pendulum portion of the FBD:

$$J\ddot{\theta} + B\dot{\theta} + K\theta - mgl \sin(\theta) - ml\ddot{x} \cos(\theta) = 0 \quad \text{where } J = I_g + ml^2$$

For a complete derivation, refer to Appendix A.

An estimate for the mass moment of inertia,  $I_g$ , for the test pilot and HTD were calculated from anthropometric tables [20] and literature on the HTD [14], respectively. The anthropometric tables are based upon measurements of unimpaired adult males and cadavers. Segment masses are expressed as a percentage of total body mass. The test pilot has decreased mass in the lower extremities and increased upper body mass from manual wheelchair propulsion. Therefore, accepting values directly from the tables based upon the total mass of the test pilot may lead to poor estimates. An “adjusted” mass of 65kg [21] was adopted for use with anthropometric tables. The tables also provide the center of gravity and radius of gyration as a function of segment length. These values in conjunction with kinematic data and implementation of the parallel axis theorem allowed the determination of the composite center of gravity and mass moment of inertia of the inverted pendulum.

The inertial term, gravity term, and wheelchair acceleration term are collected together on the right side of the equation to form a forcing function,  $\tau_{(t)}$ . B and K are constants and satisfy the equation:

$$[B \quad K] \cdot \begin{bmatrix} \dot{\theta}_{(t)} \\ \theta_{(t)} \end{bmatrix} + e_{(t)} = \tau_{(t)}$$

where  $\theta_{(t)}$ ,  $\dot{\theta}_{(t)}$ , and  $\tau_{(t)}$  are the angular displacement, velocity, and forcing torque at an observation in time, t.  $e_{(t)}$  is the residual from the fitted model at time t. B and K were determined by least-squares regression. To prevent biasing the estimate with data from the start of the trial, where the input from the wheelchair is nearly zero, and from the end of the trial, after the system has come to rest, parameters were calculated from the initiation of the braking condition to the time at which the wheelchair acceleration magnitude settled to less than .05

m/s<sup>2</sup>. Average values of B and K were determined from four trials within each speed/braking condition. As B and K are dynamic coefficients, pairing is not necessary. Hence, statistical comparisons were performed using student t-tests.

### 3.0 RESULTS

Table 2 displays the speed of the power wheelchair for each speed/braking condition as well as the trunk kinematics of the test cases. Figures 11-13 present sample curves of the trunk angular displacement, velocity, and acceleration of the test cases during emergency power off braking and the fast initial wheelchair speed.

**Table 2** The means  $\pm$  (SD) of the wheelchair speed at brake initiation, trunk angular displacement (TAD), velocity (TAV), and acceleration (TAA) are compared between the Hybrid III (HTD) and test pilot (TP) for the three braking conditions, joystick release (JR), joystick full reverse (FR), and emergency power off (EPO). No statistical differences were present between the TP and HTD for all measures.

Trial	Speed (m/s)		TAD ( $^{\circ}$ )		TAV ( $^{\circ}$ /s)		TAA ( $^{\circ}$ /s $^2$ )	
	TP	HTD	TP	HTD	TP	HTD	TP	HTD
Slow JR	.75 (.01)	.76 (.01)	4.0 (1.5)	5.9 (0.3)	24.1 (4.9)	29.6 (1.5)	247 (43)	263 (24)
Slow FR	.75 (.01)	.76 (.01)	8.4 (2.9)	9.2 (0.9)	25.3 (4.9)	34.2 (2.4)	262 (34)	287 (19)
Slow EPO	.72 (.01)	.76 (.01)	13.1 (8.0)	9.2 (0.9)	36.1 (9.1)	40.5 (3.5)	327 (45)	348 (28)
Med JR	1.54 (.05)	1.38 (.00)	3.6 (2.4)	5.3 (0.7)	13.1 (5.7)	22.9 (3.5)	155 (52)	189 (44)
Med FR	1.58 (.02)	1.38 (.01)	4.1 (1.6)	6.3 (0.9)	13.1 (5.7)	24.8 (4.9)	217 (62)	219 (35)
Med EPO	1.56 (.01)	1.38 (.02)	13.6 (2.0)	18.7 (6.1)	29.3 (3.2)	40.1 (7.5)	302 (23)	344 (39)
Fast JR	1.96 (.01)	1.97 (.01)	2.1 (0.7)	9.6 (0.8)	14.8 (2.4)	22.3 (1.2)	189 (29)	148 (47)
Fast FR	1.97 (.02)	1.98 (.01)	57.7 (37.6)	52.5 (25.2)	90.1 (56.5)	62.2 (22.7)	350 (136)	230 (24)
Fast EPO	1.95 (.03)	1.97 (.01)	83.2 (1.2)	66.5 (0.6)	185.7 (24.9)	117.7 (5.7)	564 (59)	377 (56)

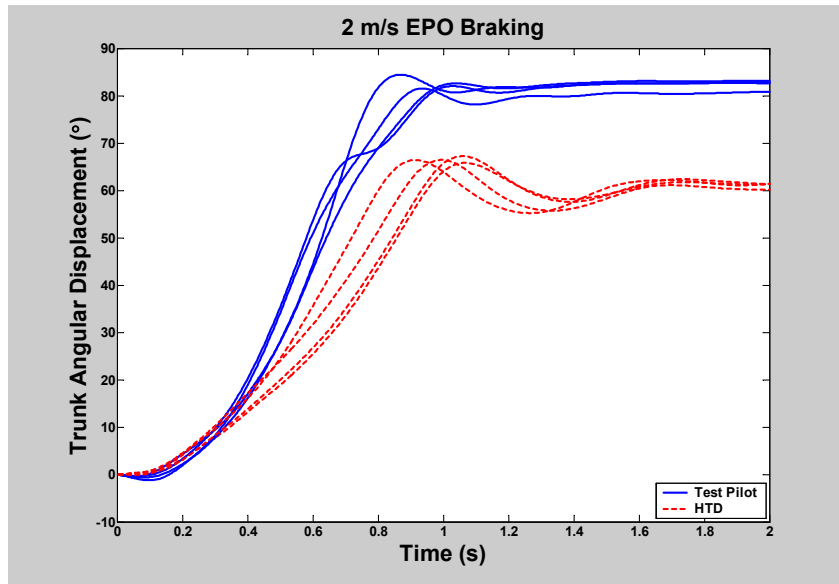


Figure 11 Trunk angular displacement of the test pilot and HTD during 2m/s, emergency power off braking.

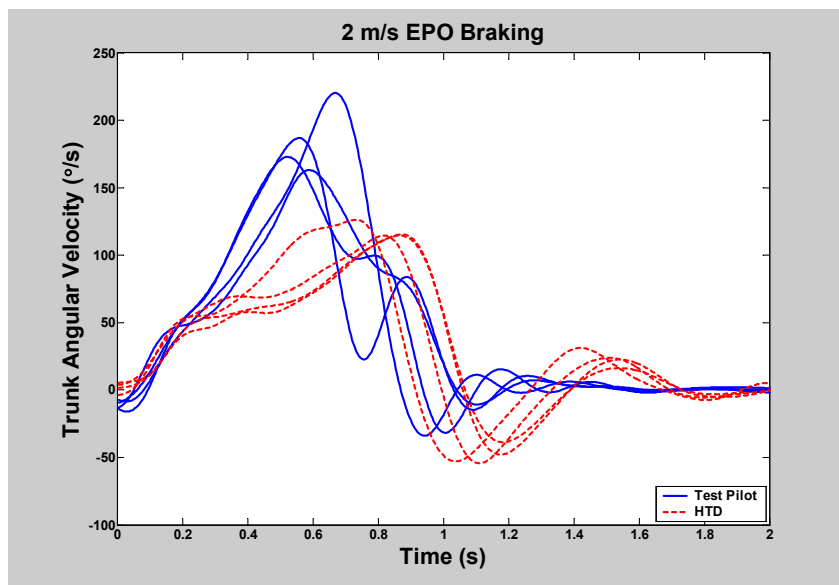
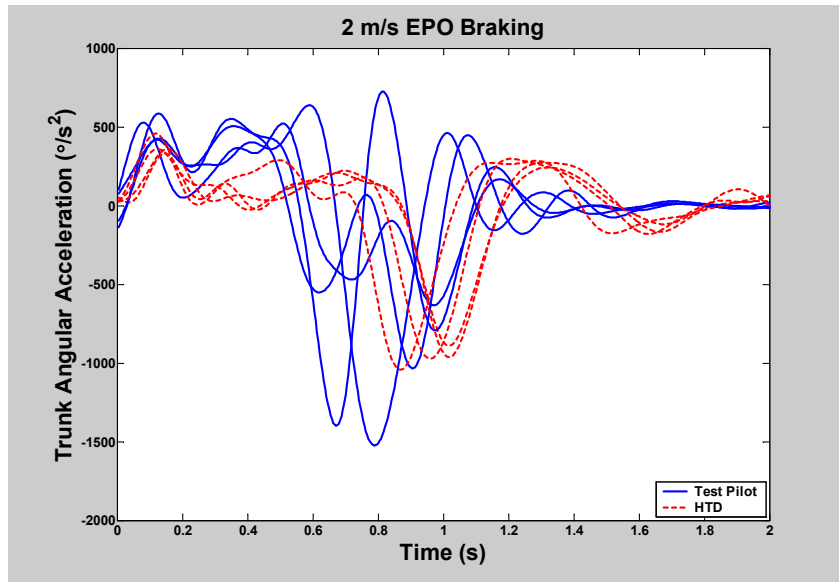


Figure 12 Trunk angular velocity of the test pilot and HTD during 2m/s, emergency power off braking.



**Figure 13** Trunk angular acceleration of the test pilot and HTD during 2m/s, emergency power off braking.

No statistical differences ( $p=.163$ ) were found in the wheelchair speed at brake initiation regardless of the rider. Analysis of the trunk angular displacement between the test pilot and HTD revealed no statistical differences ( $p=.867$ ). No significant differences were present in the trunk angular velocity ( $p=.608$ ) and trunk angular acceleration ( $p=.408$ ) between test cases. Inspection shows at the slow and middle speeds the motion of the HTD meets or exceeds the motion of the test pilot. However, at the fast speed, full reverse and emergency power off braking conditions, the HTD slightly underestimates the motion of the test pilot. Unfortunately, these are conditions that produce the highest wheelchair accelerations and possibly greatest risk of a fall. Also note that the standard deviations of the kinematic parameters were much greater during the fast speed, joystick full reverse braking condition. This is addressed in the discussion.

Table 3 lists model parameters of the test pilot and HTD. The upper extremity masses of the test pilot and HTD were estimated at 44.07 and 42.01 kg, respectively. The length of the pendulum, or distance from the hip joint center to the center of gravity of the upper body was

.2990 ± .0110 m for the test pilot and .2645 ± .0095 m for the HTD. A mass moment of inertia of 2.32 kgm<sup>2</sup> for the test dummy was used during calculations and a value on average of 2.06 ± .14 kgm<sup>2</sup> for the test pilot. The dynamic model produced estimates for the damping coefficient, B, of 27.15 ± 14.04 Nms (or kgm<sup>2</sup>/s) for the test pilot and 18.66 ± 4.59 Nms for the HTD. A t-test showed these were not statistically different (p=.115). Model estimates for the stiffness, K, were 106.09 ± 11.81 and 101.40 ± 18.25 Nm for the test pilot and surrogate rider, respectively. These were not statistically different as well (p=.528).

**Table 3 Model parameters of the test pilot and HTD.**

	m (kg)	l (m)	I <sub>g</sub> (kgm <sup>2</sup> )	B (Nms)	K (Nm)
Test Pilot	44.07	.2990 (.0110)	2.06 (.14)	27.15(14.04)	106.09 (11.81)
HTD	42.01	.2645 (.0095)	2.32 (0)	18.66 (4.59)	101.40 (18.25)

## **4.0 DISCUSSION**

The ultimate goal of the development of a low-speed, low-impact test dummy is to reduce wheelchair accident frequency and severity. A first step in this goal is the development of a robust test device that provides accurate and repeatable data relevant to the population being studied.

### **4.1 Kinematic Comparison**

To insure that comparisons between the test pilot and HTD are valid, the speed of the wheelchair when braking was initiated for each test case was compared. Changing the initial speed and braking conditions was done to introduce variation into the outcome variables. If changing the speed and/or braking condition (deceleration) had no impact on the motion of the test cases, this would indicate that the dependent variable is independent with respect to the test variables, and hence there would be no method (within the scope of this study) of influencing it, and interventions other than speed and deceleration would be necessary for reducing the incidence of tips and falls. It is important that the variation that is added is the same regardless of the rider. The speed of the wheelchair at brake initiation for the test pilot and HTD was not significantly different which indicates that the latter is the case. Note that the speeds were very similar between test cases and had small standard deviations with the exception of the medium speed. The observed difference in speed is likely because testing occurred on two different days, the first with the Hybrid III test dummy and the second with the test pilot. The medium speed had to be retuned in between tests. As the potentiometer is sensitive to small movements, bumping the speed dial accidentally can produce differences in speed.

The trunk displacement was found to be similar over a range of wheelchair speeds and decelerations. This is promising evidence that the test dummy can be a suitable surrogate for a wheelchair user in low speed dynamic studies. The trunk angular velocity and acceleration were not statistically different. This may indicate that the test cases have similar characteristics and anthropometrics. Repeatability is an important feature of a test device. The motion curves in Figures 10-12 are similar to each other in magnitude, shape, and phase. This is partly supported by the small standard deviations of the peak values. The larger standard deviations of the kinematic parameters noticeable during the fast speed, joystick full reverse braking condition are due to the number of trials in which the test cases fell forward. In three of the four trials, the test cases fell forward. In the remaining trial, the test case displaced forward, but did not fall over, and returned to rest on the seatback. This occurred for both test pilot and HTD and may be further qualitative evidence that the HTD is a suitable surrogate for wheelchair testing. Table 4 summarizes qualitatively the level of trunk stability of the test cases. Since no falls occurred during the study, the occurrence of loss of controls was reported. A loss of control was defined as the event when the wheelchair rider falls forward but remains in the chair in a position that would make operating the wheelchair difficult.

**Table 4 “Loss of controls” experienced by test cases during braking trials.**

Speed	Braking Condition	Test Pilot	HTD
.8 m/s	JR	0/4	0/4
	FR	0/4	0/4
	EPO	0/4	0/4
1.4 m/s	JR	0/4	0/4
	FR	0/4	0/4
	EPO	0/4	0/4
2.0 m/s	JR	0/4	0/4
	FR	3/4	3/4
	EPO	4/4	4/4

## 4.2 Dynamic Model

The estimated values of the damping constant,  $B$ , and stiffness constant,  $K$ , were statistically similar for the HTD and test pilot. Before conclusions can be drawn about the degree to which motion, and hence underlying characteristics, of the HTD matches that of the test pilot, it is prudent to check the closeness of the model to the actual data. A simple statistic is the coefficient of determination,  $R^2$ . It measures the fraction of the total variability in the data that is accounted for by the model. The coefficient of determination was  $.533 \pm .204$  for the test pilot and  $.760 \pm .112$  for the HTD. The model appears to describe the motion of the HTD better than the test pilot. This is not surprising considering the HTD is passive and is comprised of metals and rubber and other engineering materials that model well, contrasted to the test pilot with soft tissues, internal organs, muscles, tendons, and ligaments as well as active muscle components.

Unfortunately, a high coefficient of determination does not guarantee a close match between the model output and the measured response. Consider two sinusoids of different amplitude. Their correlation would be one but the difference in magnitude of the curves could be significant. It is arguable that a test dummy with motion highly correlated to that of a wheelchair user is sufficient for test purposes. However, limited insight would be provided into injury mechanisms since data acquired from instrumentation could not be directly compared to injury criteria. Rather an inverse dynamics or other approach to scale inertial and impact loads measured by instrumentation would be necessary and calibration for this process may be difficult to validate. A more practical solution is to develop a test dummy with similar kinematics, anthropometrics, and surface properties. This will produce realistic impact loadings already associated with injury. In cases of people with spinal cord injuries, considerable changes to the lower extremities occur. There are no published impact injury criteria for people with

disabilities. It is possible to modify injury criteria for fractures of the femur and tibia based on research investigating changes in bone density and geometry changes after spinal cord injury [22-26].

Graphical analysis of the residuals is another tool for measuring how well the model fits the data. If the errors between the model and the observed response appear to behave randomly, then the model fits the data well. A residual with a non-random structure indicates the model fits the data poorly. Graphs of the residuals versus the model parameters,  $\theta$  and  $\dot{\theta}$ , were created and included in Appendix B. Errors from the fitted test pilot modeling showed an increase in variance as the cog angular displacement increased. The residual from the HTD modeling was small in comparison to the residuals from the test pilot modeling but exhibited a pattern. A pattern of underestimation can be seen from  $-10$  to  $20$  degrees followed by a period of overestimation from  $20$  to  $50$  degrees. The variance rose sharply around  $50$  to  $60$  degrees possibly indicating an event that the model did not describe well. No patterns were evident in plots of the errors versus the cog angular velocity. Errors versus the cog angular velocity plots gave no indication that the model parameters were of incorrect form. The graphical analysis indicates that the functional form of the model may be incorrect. The mismatch could occur from variables in the function that were omitted, variables which were included that do not belong, and states that the model cannot address.

A limitation is that the model does not consider collisions between the rider's upper body and the legs or other parts of the wheelchair. These collisions represent discontinuities that a continuous model does not address well. Body collisions impart a large force that is not considered in the forcing input. Energy lost during the collisions is not accounted for, thus biasing estimate for B and K. Results of the trunk angular displacement indicated that this

occurred in at least 6 of the 36 trials of the test pilot and none of the trials involving the HTD.  $R^2$  values were high for these trials ( $R^2 \approx .8$ ).

The backrest normal force is not considered by the model and may lead to inaccuracies in estimates of the dynamic coefficients. Before the braking condition was initiated, and hence the disturbance of the wheelchair/rider system, the test pilot and HTD were reclined in the seat such that the angle between the vertical and the hip to center of gravity vector was about  $16^\circ$  and  $10^\circ$ , respectively. In this quasi-static situation, the wheelchair speed at this point is nearly constant, therefore, the wheelchair acceleration,  $\ddot{x}$ , is approximately zero. The angular displacement,  $\theta$ , of the test cases was nearly constant as well meaning the time derivatives,  $\dot{\theta}$  and  $\ddot{\theta}$ , are very small, leading to an approximation of K to be:  $K = mgl \sin(\theta) / \theta$ .

The model would conclude that the torque provided by the spring would equal the moment caused by the weight of the upper body about the hip. This results in initial estimates of 128 and 107 Nm for the test pilot and HTD, respectively.

The normal force of the backrest on the rider could be accounted for. If it was considered at the onset of the study, the wheelchair could be instrumented for measurement of the normal force. Unfortunately, this was not done. It could be included in the model as a spring with only stiffness in compression (or tension for that matter). The spring would be loaded by the weight of the rider leaning on the backrest. The spring would return energy to the pendulum until it reached the zero displacement, or the event in which the rider's back no longer contacted the backrest. In this case because the displacement of the rider and the backrest are about the same in this range, the springs could be considered in parallel. Their equivalent stiffness would be  $K_{eq} = K_1 + K_2$ . It is possible that the model has estimated stiffness and damping values for a wheelchair/rider system rather than only the rider. Figure 14 supports this.

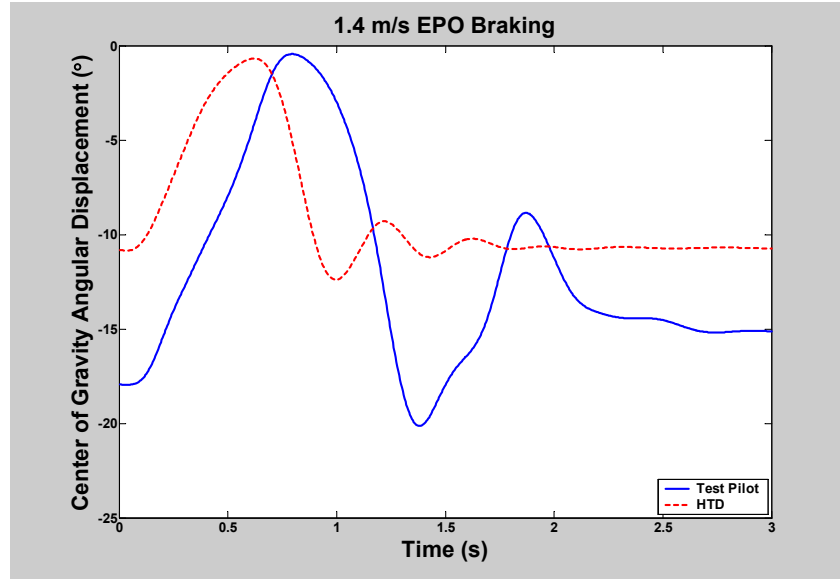


**Figure 14** Center of gravity angular displacement for one trial of the test pilot and HTD during the middle speed, emergency power off braking.

Figure 14 shows the cog angular displacement for one trial of the test pilot and HTD during the middle speed, emergency power off braking. This motion is typical in trials with slower speeds and lower wheelchair accelerations in that the center of gravity of the pendulum does not or barely reaches vertical. The oscillations that can be seen are influenced by the backrest acting as a spring. Note the period of oscillation is shorter for the HTD.

Caution must be used with models involving displacement variables. Displacement variables (stiffness,  $K\theta$ ) must be expressed with respect to some reference. Often this reference is chosen such that the “spring” is neither stretched nor compressed when the displacement variable is zero. For this model, the displacement variable was zero when the center of gravity of the inverted pendulum was directly above its fulcrum. This drawback can be remedied provided the zero displacement position of the spring is known. The dynamic equation would simply be:

$$J\ddot{\theta} + B\dot{\theta} + K(\theta - \theta_o) - mgl \sin(\theta) - ml\ddot{x} \cos(\theta) = 0$$

where  $\theta_o$  is the angle of the pendulum when the spring has zero displacement. In theory, this adjustment is simple. In practice, this reference point is difficult to determine and may vary as a function of knee angle. The stiffness of the hip is a function of knee flexion as well, further complicating the issue. Future modeling should include this influence. Currently, the model does not distinguish between hip flexion and trunk flexion. Initially, it was speculated that a simple model considering only the net angle formed by the upper body center of gravity, the hip joint center, and the vertical would be adequate for comparison of physical characteristics. A more complex model involving a double pendulum consisting of either two rotational or a rotational and a cantilever spring type pendulum or flexible elements (multiple inverted pendulums) would more realistically simulate the hip joint and trunk.

A model parameter that was not considered for the test pilot stiffness is an applied torque. The torque could be a constant value determined through empirical testing, or perhaps a ramp function that would increase as the rider became more cognizant of the risk of falling. Depending on the level of injury, no torque may be required. But this is not necessary. It is understood that the test dummy has no active movement component and therefore could never model that aspect of the test pilot. Note as well, that the test pilot is only one sample from the wheelchair user population. The population most at risk to tips and falls may have a higher spinal cord lesion and less trunk stiffness than that of the test pilot.

In general, both the test pilot and HTD exhibited an all or none response. There appears to be a critical threshold once crossed that results in a loss of control. This threshold is approximately 10° to 15° angle of the upper body center gravity from the vertical. This is in agreement with typical concepts of an inverted pendulum. The inverted pendulum is inherently unstable and has two stable points at top and bottom center. The latter is not an option for safe driving. The

problem of preventing falls or a loss of control simplifies to avoiding decelerations and slopes that create a forcing torque large enough to cause displacements that exceed the threshold. This can be achieved in a clinical environment by performing braking tests, with spotters, during the fitting process. The maximum speed and deceleration of the wheelchair can be programmed until a loss of control does not occur. There is a trade-off between functional posture and safe driving posture that a clinical professional is required to make.

The HTD appears to exhibit some damped harmonic motion. The HTD has a mechanism as well for storing energy as a function of displacement. The test dummy has a polyacrylate lumbar spine that is flexible and provides stiffness and some damping properties. As noted earlier, the HTD exhibits similar oscillatory motion at the lower speed, lower deceleration trials as the test pilot, but with higher frequency. This can also be seen on Figure 11 although less noticeable because of the scale. Figure 15 is an enlarged view of the end of the trials in Figure 11.

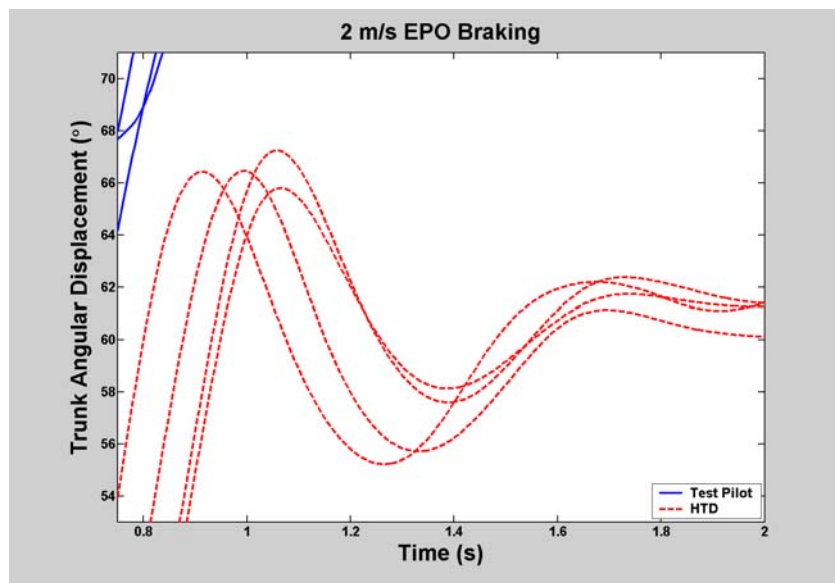


Figure 15 Center of gravity angular displacement of the test pilot and HTD near the end of the 2 m/s emergency power off braking trials.

The period of the oscillations is about the same in each picture. The spring in this case seems to have a zero displacement that corresponds with a trunk angle of about 60°. The differences in the kinematics noticed at the fast speed and emergency power off braking condition is attributed to an impingement occurring between the pelvis and thighs of the HTD. When the impingement occurs, trunk flexion via the hips stops and the inertia of the upper body causes the test dummy to continue to bend, only at the lumbar spine. Removing the source of the impingement will increase the similarities further between the HTD and test pilot.

The HTD as presented in this study is appropriate for investigating wheelchair setup (legrest adjustment, seat angle, etc.) and environmental factors (curbs, curb cuts, ramps, etc.) that may influence occupant safety. The motion of the HTD matches that of the test pilot in most cases. There is a possibility at the fastest speed and most severe braking condition that the HTD may underestimate the severity of occupant excursion. This suggests that results obtained from testing with the dummy, i.e. falls, injuries, would likely occur to a wheelchair user under the same conditions. However, there may be some injuries or falls that the test dummy may not detect. The most critical factors influencing safety, however, would likely still be identified. A possible source of the underestimation has been identified and immediate steps should be taken to remove the interference in the HTD legs to provide more motion in the hips. Caution should be taken when evaluating wheelchair setup features since these may involve changing the posture of the dummy and the influence of knee flexion on hip stiffness has not been used as a point for validating the HTD.

The dynamic model determined consistent values for damping and stiffness coefficients; however, it is likely the model estimated properties for a wheelchair/rider system rather than only the rider. The properties determined provide first estimates for dynamic simulation software to perform virtual testing.

## APPENDIX A

### DERIVATION OF EQUATIONS OF MOTION FOR CART WITH AN INVERTED PENDULUM SYSTEM

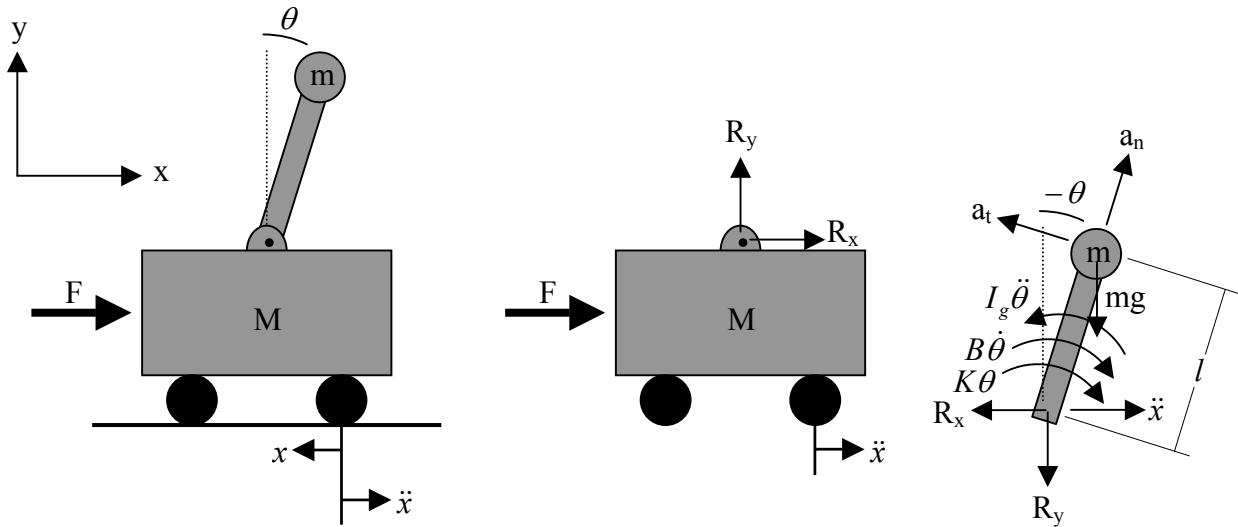


Figure 16 Free body diagrams of cart with an inverted pendulum system.

A “right-hand” Cartesian coordinate system is used. Staying consistent with this description, positive moments are defined as counter clockwise or in the direction of  $x \times y$ . Displacement of the cart,  $x$ , is in the  $-x$  direction. A braking force,  $F$ , is applied to the cart, causing it to decelerate (or accelerate in the direction of  $\ddot{x}$ ). The moments  $I_g \ddot{\theta}$ ,  $B \dot{\theta}$ , and  $K \theta$  are drawn on the free body diagrams oriented in the positive direction. This is not necessarily the direction of those moments for the figure shown above. The direction of  $\theta$ ,  $\dot{\theta}$ , and  $\ddot{\theta}$  address the direction of the moments. The angle of the pendulum is measured with respect to vertical. Clockwise displacements are considered negative and counter clockwise displacements positive. This is important later when a sign change will be necessary.

To get the equation of motion of the inverted pendulum, start by summing the forces perpendicular to the pendulum:

$$\sum F_x = ma$$

$$(1) \quad -R_x \cos \theta + R_y \sin \theta + mg \sin \theta = -ma_t + m\ddot{x} \cos \theta$$

To eliminate the reaction force terms,  $R_x$  and  $R_y$ , from the above equation, sum the moments around the center of gravity of the pendulum.

$$\textcircled{+} \sum M_g = I_g \alpha$$

$$(2) \quad -R_x l \cos \theta + R_y l \sin \theta - B \dot{\theta} - K \theta = I_g \ddot{\theta}$$

Multiply equation (1) by  $l$ , and subtract equation (2) using linear combination to get:

$$(3) \quad mgl \sin \theta + B \dot{\theta} + K \theta = -mla_t + ml\ddot{x} \cos \theta - I_g \ddot{\theta}$$

Recall that the tangential acceleration is:

$$a_t = \alpha \times r \quad \text{where } \alpha = \frac{d^2 \theta}{dt^2} = \ddot{\theta}$$

$r$  is the vector from the fulcrum to the center of gravity of the pendulum.  $r$  has magnitude,  $l$ . Therefore  $a_t$  has magnitude  $\ddot{\theta}l$  and by the right-hand rule,  $\alpha \times r$  is in the direction of  $a_t$ .  $a_t$  can then be expressed in terms of existing variables. Moving all terms to the left side of the equation and substituting for  $a_t$  yields:

$$(4) \quad I_g \ddot{\theta} + B \dot{\theta} + K \theta + mgl \sin \theta + ml^2 \ddot{\theta} - ml\ddot{x} \cos \theta = 0$$

The parallel axis theorem states that if the moment of inertia of a body about an axis passing through the center of gravity is known, then the moment of inertia about any other parallel axis can be determined. For the pendulum above and a parallel axis distance  $l$  from the center of gravity, the moment of inertia would be:

$$J = I_g + ml^2$$

Simplifying eq. (4) with this leads to:

$$(5) \quad J \ddot{\theta} + B \dot{\theta} + K \theta + mgl \sin \theta - ml\ddot{x} \cos \theta = 0$$

Recall from above, clockwise displacements have negative sign. However, the derivation leading up to eq. (5) considered only an angle and not a displacement. Note that:

$$\sin(-\theta) = -\sin(\theta) \text{ and } \cos(-\theta) = \cos(\theta)$$

Therefore changing the sign of the  $mgl \sin \theta$  term will make eq. (5) compatible with the FBD yielding:

$$(6) \quad J\ddot{\theta} + B\dot{\theta} + K\theta - mgl \sin \theta - ml\ddot{x} \cos \theta = 0$$

## APPENDIX B

### GRAPHICAL RESIDUAL ANALYSIS

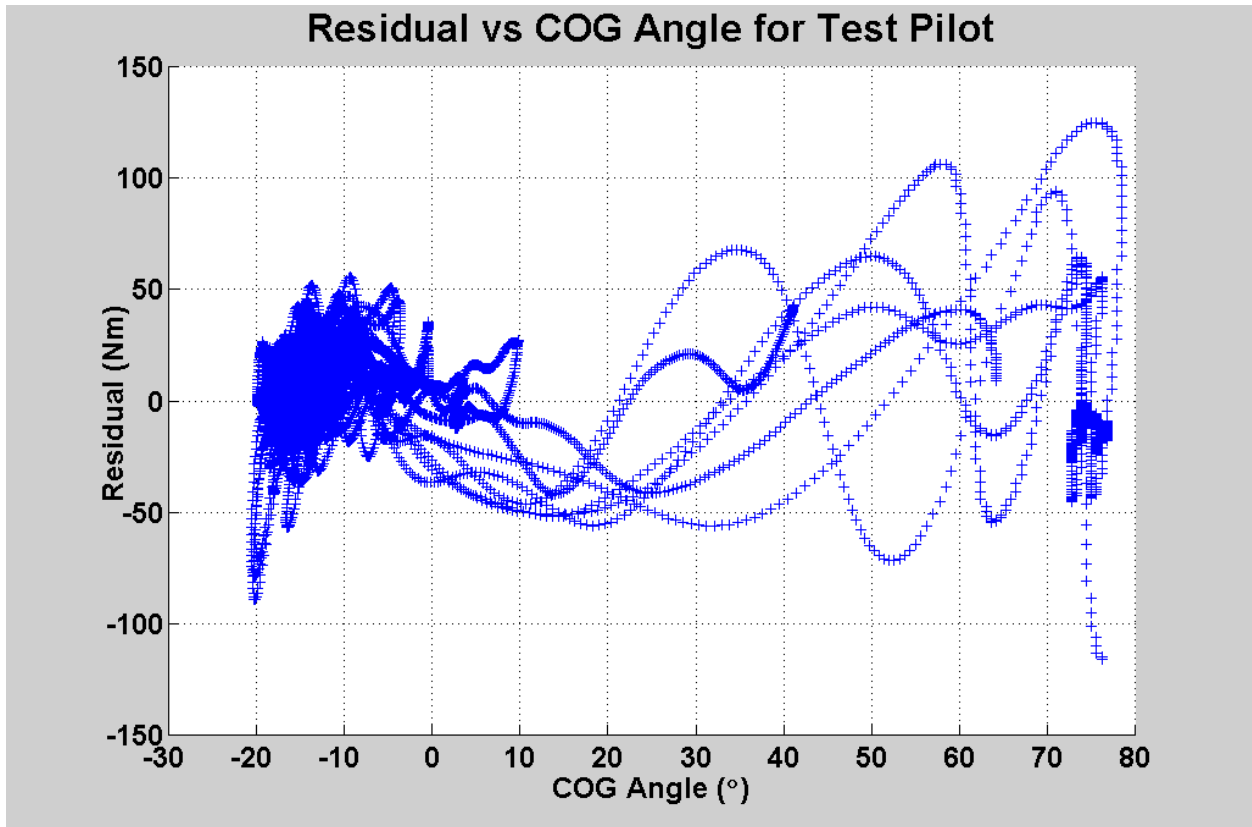


Figure 17 Residual from all trials involving test pilot vs. the model parameter, center of gravity angle.

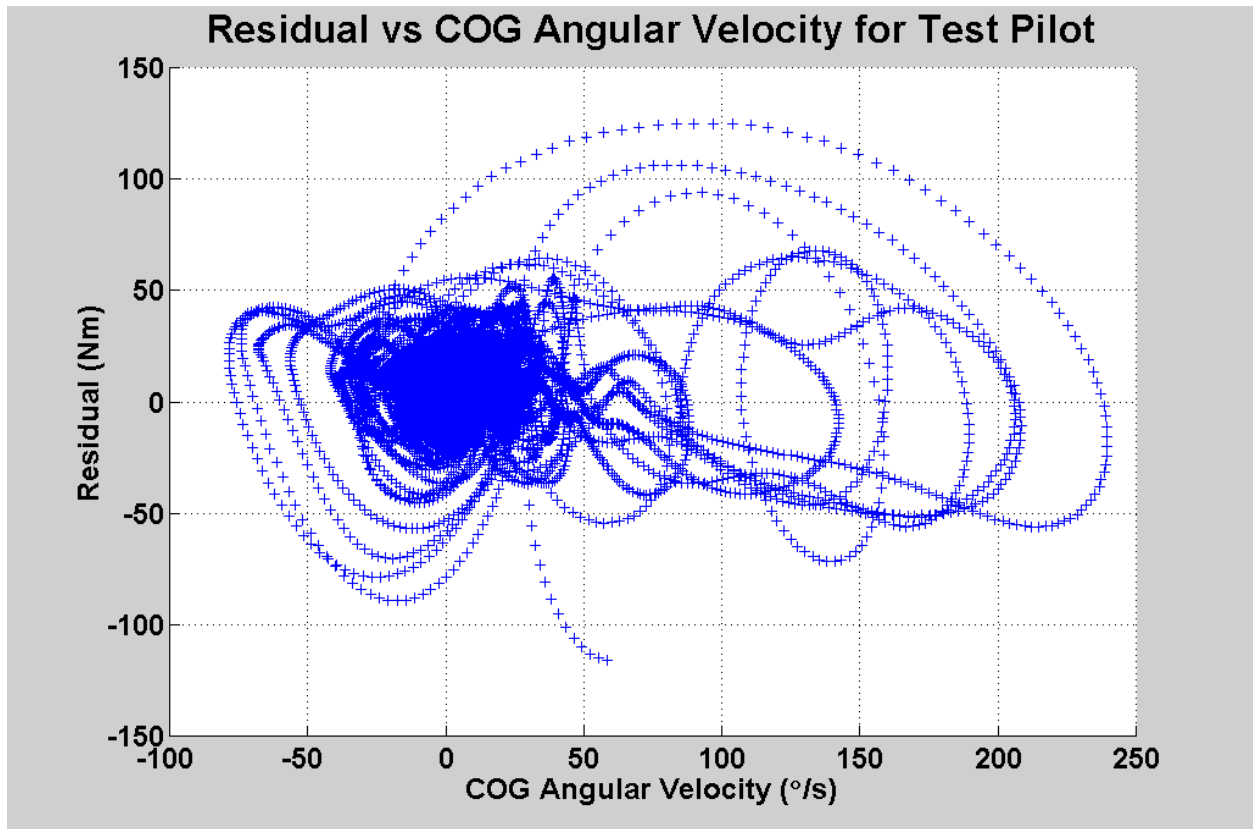


Figure 18 Residual from all trials involving test pilot vs. the center of gravity angular velocity.

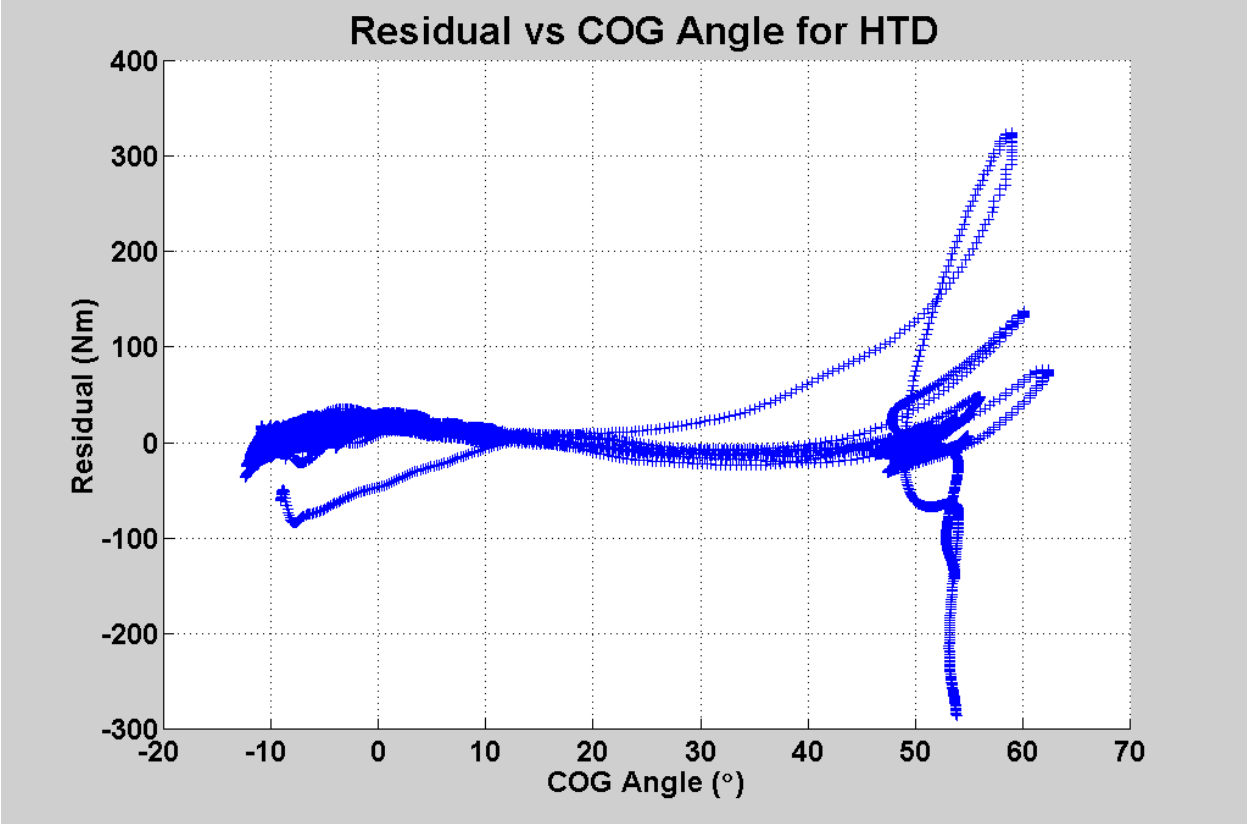


Figure 19 Residual from all trials involving HTD vs. the model parameter, center of gravity angle.

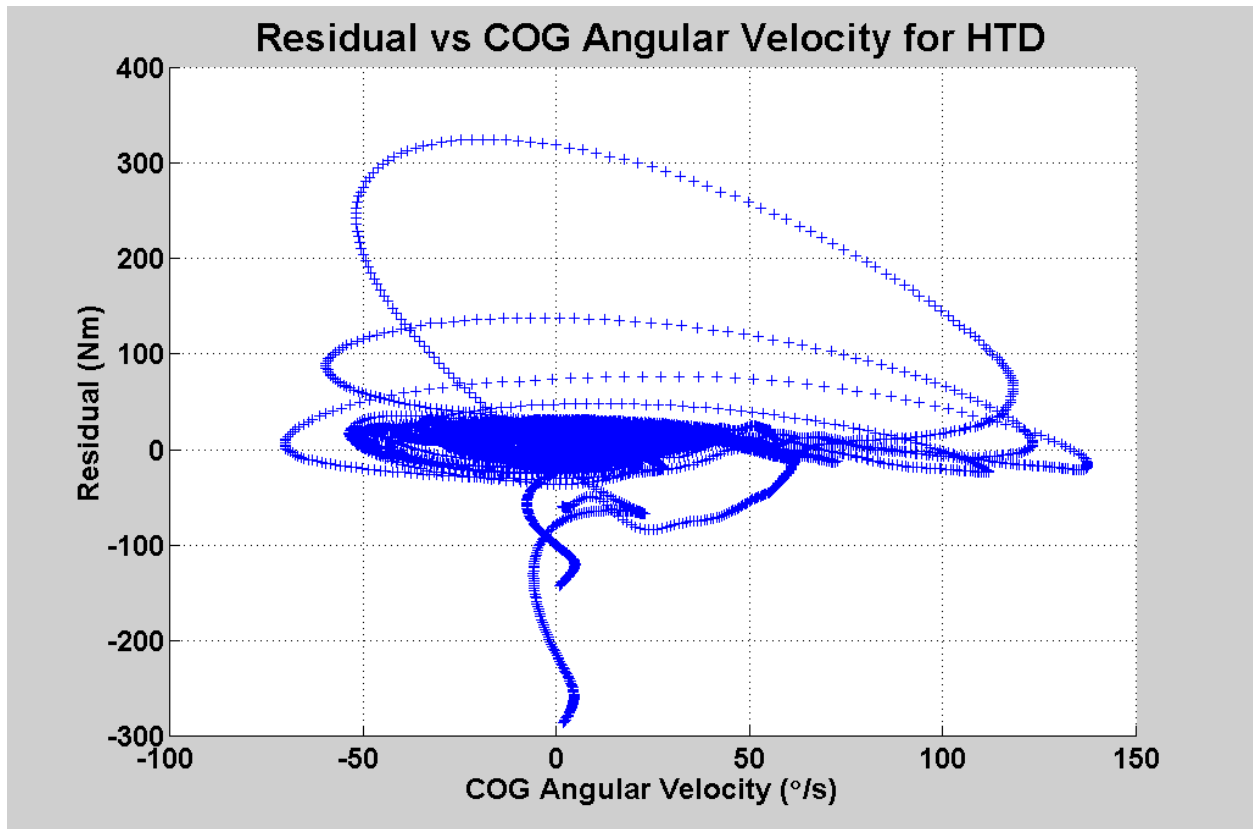


Figure 20 Residual from all trials involving HTD vs. the center of gravity angular velocity.

## APPENDIX C

### COMPOSITION OF FORCING VARIABLE

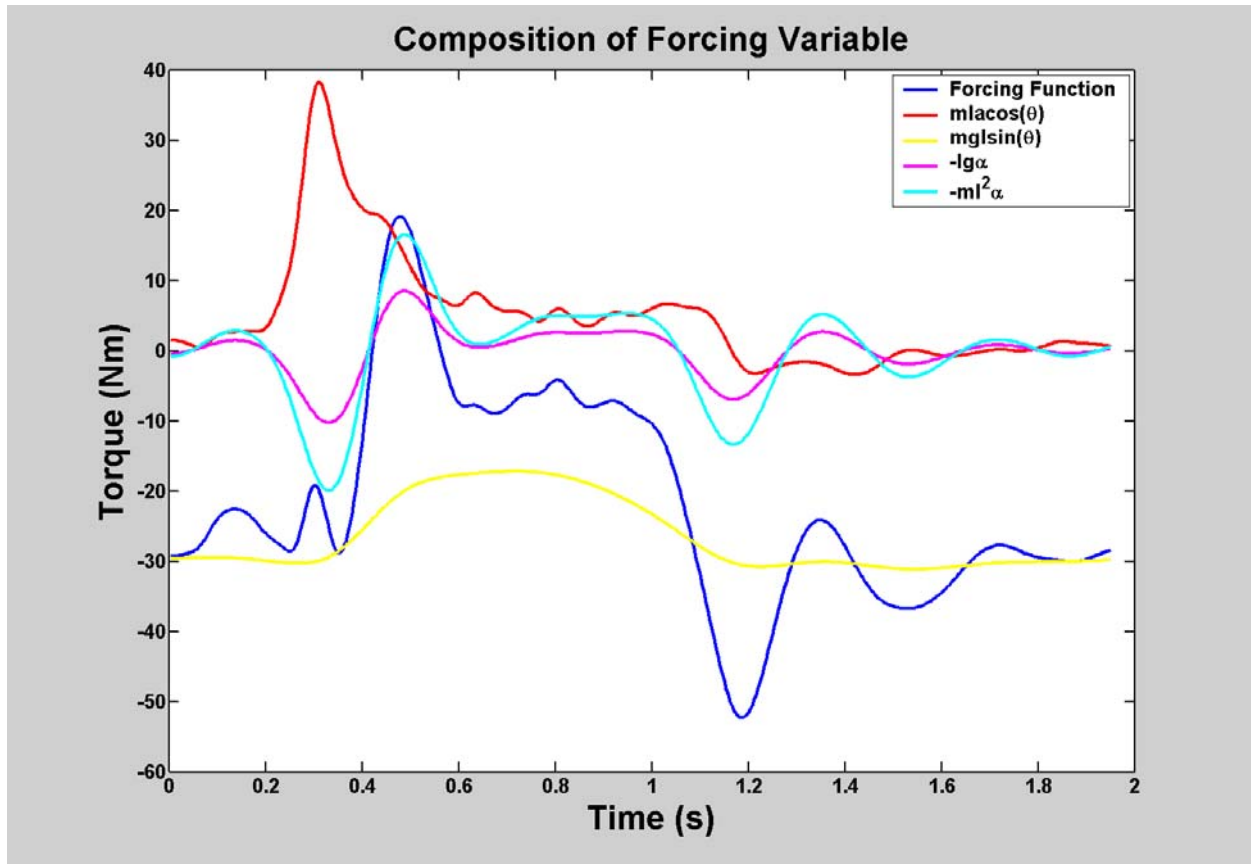


Figure 21 Composition of forcing variable.

## APPENDIX D

### MATLAB PROGRAMS

```
function batch532
%batch program written for matlab5.3
%will process every file in a selected directory
%through the selected m-file.
%will only work if path to m-file is contained in the matlabrc.m file
%or can add more directory changes in for loop
% version 5.3.2
% made filenames global so other programs can save

global f

[mfilename,file_path]=uigetfile('*.m','Select m-file to batch process with');
mfilename=strtok(mfilename, '.');

[batchdir,dir_path]=uigetfile('*..*', 'Select file in batch directory');

cd \
eval(['cd ',dir_path]);

file_list=dir;

for i=3:length(file_list)
    f=file_list(i,1).name
    load(f);
    temp=eval(strtok(f, '.'));
    eval([mfilename '(temp)']);
end;
```

```

function truncate(datar)
%eliminates missing points from beginning of
%OPTOTRAK files. For use with "batch532.m".
%To use as stand alone program, use an input
%to obtain the filename.

global f %global variable containing filename

[r,c]=size(datar);
for i=2:3:c %count by 3's, need only check 1 dir.
    jerry(i)=min(find(datar(:,i)>-10000));
end;

jerry=jerry(2:3:c);
startpoint=max(jerry);

datar=datar(startpoint:r,:);

f=[f '.trn'];

eval(['save ' f ' datar -ascii'])

```

```

function [newdata]=qksweep5(data)
%Cubic spline interpolation for missing OPTOTRAK
%markers. Uses "good" data to create a look-up
%table for interpolation. Method (linear, cubic,
%etc. can be set differently for each direction.

[R,C]=size(data);
home
disp('this could take a while'); %flowers to tell you
pause(1) %algorithm is running
home %unnecessary
newdata(:,1)=data(:,1);
flag=0;
for i=2:C

disp('percent complete')
percent=round(100*i/C);
disp(percent)

x=find(data(:,i)>-2*10e10); %define and find good points
p=find(abs(diff(data(:,i)))>13);%refine def. based upon marker vel.
p=p+1;
x=setdiff(x,p); %exclude elements p from the set x
y=data(x,i);
time=1:1:R; %an index place holder
time=time';

if ~rem(i-2,3)
newdata(:,i)=interp1(x,y,time,'spline'); %use spline for 2,5,8,...
else
newdata(:,i)=interp1(x,y,time,'cubic');
end;
%newdata3(:,i)=interp1(x,y,time,'v5cubic');

eval(['figure(' num2str(i) ')'])
plot(newdata(:,i),'r') %plot splined data
pause(.1)
axis manual
hold on

plot(data(:,i)) %plot original data containing missing points
hold on
home

end;

if newdata==data
disp('No change during sweep')
else
disp('Changes made, save file')
%[i,j]=find(newdata~=data);
end

```

```

%function dynahtdI3
%calculates all study variables for HTD

clear

[cda,cda_path]=uigetfile('*.cln', 'Select data file');
name=cda;
name=strtok(name, '.');
cda_string=[cda_path, cda];
load (cda_string);
data=eval(strtok(cda, '.'));

startx=input('enter starting frame: ');

%****define constants****
hmtranslate=[20.5 -30.5]; %hip marker translation to hip joint center
theta=6.123*pi/180;
R=[cos(theta), -sin(theta); sin(theta), cos(theta)]; %a rotation matrix
stretcher=[.556,0;0,1]; %stretches a vector by .556 in the x-dir
Rtemp=[0,-1;1,0]; %90 degree rotation matrix
m=42.01 %mass (kg)
Ig=2.3157; %mass moment of inertia (kgm^2)

%****do some initial filtering****
[D,C] = butter(2,6/120);

for i =2:10 %shoulder through knee markers
    data(:,i)=filtfilt(D, C, data(:,i));
end

%****define variables****

shoulder=[data(:,2),data(:,3),data(:,4)];

hip=[data(:,5),data(:,6),data(:,7)];

knee=[data(:,8),data(:,9),data(:,10)];

ear=[data(:,11),data(:,12),data(:,13)];

framec=[data(:,14),data(:,15),data(:,16)]; %corner of PWC frame
framef=[data(:,17),data(:,18),data(:,19)]; %front of PWC frame
joystickl=[data(:,20),data(:,21),data(:,22)]; %joystick low
joystickh=[data(:,23),data(:,24),data(:,25)]; %joystick high

%****get hip joint center****
L=length(hip)
for i=1:L
    hipjc(i,:)=[hip(i,1:2)]+hmtranslate;
end

```

```

%****One multiplication, 4 things
%****1 rotate shoulder-hip vector to x-axis (aligner)
%****2 scale down by a factor (stretcher)
%****3 rotate vector to cg (rotation matrix)
%****4 undo first rotation (hanger)

temp=shoulder(:,1:2)-hipjc;
for i=1:L
    mag(i)=norm(temp(i,:));
    perpframe1(i,:)=temp(i,)/(mag(i)); %a perpframe
    perpframe2(i,:)=perpframe1(i,:)*Rtemp;
    aligner(i).r=[perpframe1(i,:);perpframe2(i,:)]; %def. of aligner
    hanger(i).r=[perpframe1(i,:) ',perpframe2(i,:) ']; %and hanger
    cgloc(i,:)=temp(i,:)*aligner(i).r*stretcher*R*hanger(i).r;
end;

cgloc=cgloc/1000; %convert mm to m

%****calculate cog angle****
theta=atan2(cgloc(:,2),cgloc(:,1))-pi/2; %pi/2 means angle w/respect to vert.
%note L*sin(theta)=cgloc(:,1)
% L*cos(theta)=cgloc(:,2)

figure(1)
plot(theta*180/pi) %plot angle of cog

thetafilt=filtfilt(D,C,theta); %filter that angle

hold on
plot(thetafilt*180/pi,'r') %plot filter cog angle

theta=thetafilt;

%****time derivatives of theta****
thetadot=ali_diff(thetafilt).*240; %cog angular vel.

figure(2)
plot(thetadot)
thetadot=FILTFILT(D, C, thetadot);
hold on
plot(thetadot,'-r')
title('cg angular vel')

figure(3)
hold on
thetaddot=ali_diff(thetadot).*240; %cog angular acc.
plot(thetaddot)
title('cg angular acc')

%****find chair acceleration****
%2 ways (but both arrive at exactly same curve)
%1
avgframe=(framec(:,1)+framef(:,1))/2000; %avg. markers to reduce noise

```

```

avgframev=ali_diff(avgframe)*240; %avg. marker velocity

[B,A] = butter(2,12/120);
avgframevfilt=filtfilt(B,A,avgframev);

figure(4)
plot(-avgframev)
hold on
plot(-avgframevfilt,'r')
title('Wheelchair Velocity')

%2 (can be commented out)
framecvx=ali_diff(framec(:,1)).*240;
framecvx=framecvx/1000;

framefvx=ali_diff(framef(:,1)).*240;
framefvx=framefvx/1000;

chairspeed=(framecvx+framefvx)/2;
filtchair=filtfilt(B, A, chairspeed);
plot(-filtchair,'m')

%1 back to one
chairacc=ali_diff(avgframevfilt)*240; %PWC acceleration
chairaccfilt=filtfilt(B, A, chairacc);

figure(5)
plot(chairacc)
hold on
plot(chairaccfilt,'r')
title('Wheelchair Acceleration')

%***find end frame (chair input -> 0)***
accbackward=flipud(chairaccfilt);
lacc=length(chairaccfilt);
accbackward=accbackward(50:lacc-50,:);
index=min(find(abs(accbackward)>.05));
endx=lacc-50-index;
plot(endx,chairaccfilt(endx),'gx')
endx

%trim down to size
theta=theta(startx:endx);
thetadot=thetadot(startx:endx);
thetaddot=thetaddot(startx:endx);
chairaccfilt=chairaccfilt(startx:endx);
cgloc=cgloc(startx:endx,:);

%***dynamic model***
l=mag'*0.556/1000;
l=l(startx:endx,:);
phi=[thetadot theta];
r=phi'*phi;

```

```

xterm=m*chairaccfilt.*1.*cos(theta); %acc. term from PWC
nonlin=m*9.8067*1.*sin(theta); %gravity term of upper body
inertial=-m*(1.^2).*thetadot; %inertial term from parallel axis
igterm=Ig*thetadot; %mass moment of inertia term
%forcing=[-m*chairaccfilt.*cgloc(:,2)      +      m*9.8067*cgloc(:,1)      -
m*1.^2.*thetadot - igterm];
forcing=[m*chairaccfilt.*1.*cos(theta)      +      m*9.8067*1.*sin(theta)      -
m*1.^2.*thetadot - igterm];

P=pinv(r)*(phi'*forcing); %pseudoinverse
P' %P' is 1x2 matrix containing B and K (damping, stiffness constants)

disp('program paused')
pause

%***Goodness of Fit***
X=P(1)*thetadot + P(2)*theta;
Y=forcing;

rho=corrcoef(X,Y);
rho=rho(1,2)

residual=(Y - X); %error in model
figure(18)
plot(residual)
figure(19) %error vs. cog angle
scatter(theta*180/pi,residual);
figure(20) %error vs. cog angular velocity
scatter(thetadot*180/pi,residual);

%***Calculate a few PWC Parameters***
speed_at_brake=-avgframevfilt(startx);

speed_95=.95*speed_at_brake;
speed_05=.05*speed_at_brake;

startframe=min(find(-avgframevfilt<=speed_95)); %find 95% and 5%
endframe=min(find(-avgframevfilt<=speed_05)); %of brake initiation speed

figure(8) %shows on graph, velocity of PWC, start of brake
plot(-avgframevfilt); %and 95% & 5% of brake initiation speed
hold on
plot(startframe,-avgframevfilt(startframe),'xg')
plot(endframe,-avgframevfilt(endframe),'xr')

%***95/5 Braking Distance***
brake_dis=-((framec(endframe,1)-framec(startframe,1))+(framef(endframe,1)-
framef(startframe,1)))/2;
%brake_dis=-(framef(endframe,1)-framef(startframe,1));

%***95/5 Braking Time***
brake_time=(endframe-startframe)/240;

```

```

%****trunk angles****
[R,Col]=size(shoulder);

hiptoshould=[shoulder(:,1)-hip(:,1) shoulder(:,2)-hip(:,2)];
hiptoknee=[knee(:,1)-hip(:,1) knee(:,2)-hip(:,2)];
for i=1:R

trunkangle(i)=acos(dot(hiptoshould(i,:),hiptoknee(i,:))/(norm(hiptoshould(i,:))
)*norm(hiptoknee(i,:)));
end

figure(9)
trunkangle=trunkangle*180/pi;
plot(trunkangle)
trunkangle=filtfilt(D,C,trunkangle);
hold on
plot(trunkangle,'-r')
offset=trunkangle(startx);
trunkdisp=offset - trunkangle;
plot(trunkdisp,'g')
title('trunk angular disp')

figure(10)
trunkvel=ali_diff(trunkdisp).*240; %trunk angular vel.
plot(trunkvel)
trunkvel=FILTFILT(D, C, trunkvel);
hold on
plot(trunkvel,'-r')
title('trunk angular vel')

figure(11)
trunkacc=ali_diff(trunkvel).*240; %trunk angular acc.
plot(trunkacc)
title('trunk angular acc')

maxtrunkdisp=max(trunkdisp);
maxtrunkvel=max(trunkvel);
maxtrunkdec=max(trunkacc);
max_acc=max(chairaccfilt);
%pause

cda_path
suggest=name;

[cda, cda_path] = uiputfile([suggest '.res'], 'Save As'); %select name and
path for saving file
cd \
eval(['cd ' cda_path]);

fid=fopen(cda,'w'); %open file for writing
fprintf(fid,'%f\t %f\t %f\t %f\t %f\t %f\t %f\t %f\t %f\t\n',P(1),P(2),speed_at_brake,maxtrunkdisp,
maxtrunkdec,brake_dis,brake_time,max_acc);
fclose(fid);

name=strtok(cda, '.');

```

```
lfile=[name '.l'];
resfile=[name '.err'];

fid=fopen(lfile,'w');
fprintf(fid,'%f\n',l);
fclose(fid);

fid=fopen(resfile,'w');
fprintf(fid,'%f\n',residual);
fclose(fid);
```

```

%function dynacoop
%calculates all study variables for test pilot trials

clear

[cda,cda_path]=uigetfile('*..*', 'Select data file');
name=cda;
name=strtok(name, '.');
cda_string=[cda_path, cda];
load (cda_string);
data=eval(strtok(cda, '.'));

startx=input('enter starting frame: ');

%****define constants****
m=65; %mass (kg)

thn=.578; %percent mass of trunk/head/neck
Uarm=.028; %percent mass of upper arm
FarmH=.022; %percent mass of forearm & hand

UEm=m*(thn+2*(Uarm+FarmH)); %Upper Extremity mass

thncog=.66; %cog/segment length
Uarmcog=.436;
FarmHcog=.682;

thnk=.503; %radius gyration/segment length
Uarmk=.322;
FarmHk=.468;
%*****

%****do some initial filtering****
[D,C] = butter(2,6/120);

for i =2:19 %shoulder through wrist markers
    data(:,i)=filtfilt(D, C, data(:,i));
end

%****define variables****

shoulder=[data(:,2),data(:,3)];

hip=[data(:,5),data(:,6)];

knee=[data(:,8),data(:,9),data(:,10)];

ear=[data(:,11),data(:,12),data(:,13)];

elbow=[data(:,14),data(:,15)];

wrist=[data(:,17),data(:,18)];

framec=[data(:,20),data(:,21),data(:,22)];

framef=[data(:,23),data(:,24),data(:,25)];

```

```

joystickl=[data(:,26),data(:,27),data(:,28)];

joystickh=[data(:,29),data(:,30),data(:,31)];

if 0
%***Get joystick angle***
s=input('do you want to get joystick angle: ')
if s
    framevector=framec-framef;
    joystickvector=joystickh-joystickl;
    %in an angle A-V-B where V is vertex
    A=[joystickvector(:,1) joystickvector(:,2)];
    B=[framevector(:,1) framevector(:,2)];
    [r,c]=size(joystickvector);
    for i=1:r

        joystickangle(i)=(180/pi)*acos(dot(A(i,:),B(i,:))/(norm(A(i,:))*norm(B(i,:)))));
    end
    %joystickangle=-joystickangle;

    figure(20)
    plot(joystickangle)
    title('joystick angle')
end
end

%***Segment Lengths***
L=length(wrist);

for i=1:L
    forearml(i)=norm([wrist(i,:)-elbow(i,:)]);
    uarml(i)=norm([elbow(i,:)-shoulder(i,:)]);
    chestl(i)=norm([shoulder(i,:)-hip(i,:)]);
end

forearml=forearml/1000; %mm->m
uarml=uarml/1000;
chestl=chestl/1000;

%***Segment CoG (from proximal)***
forearmcgloc=FarmHcog*[wrist-elbow] + elbow;
uarmcgloc=Uarmcog*[elbow-shoulder] + shoulder;
chestcgloc=thncog*[shoulder-hip] + hip;

%***Get UE CoG Location***
UEcglocx=m*(2*FarmH*forearmcgloc(:,1) + 2*Uarm*uarmcgloc(:,1) +
thn*chestcgloc(:,1))./UEm;
UEcglocy=m*(2*FarmH*forearmcgloc(:,2) + 2*Uarm*uarmcgloc(:,2) +
thn*chestcgloc(:,2))./UEm;

figure(1) %plot segments and CoG
plot(elbow(:,1),elbow(:,2))
hold on
plot(shoulder(:,1),shoulder(:,2))

```

```

plot(hip(:,1),hip(:,2))
plot(wrist(:,1),wrist(:,2))
plot(UEcglocx,UEcglocy,'o')

for i=50:50:length(shoulder)
    plot(elbow(i,1),elbow(i,2),'rx')
    plot(shoulder(i,1),shoulder(i,2),'rx')
    plot(hip(i,1),hip(i,2),'rx')
    plot(wrist(i,1),wrist(i,2),'rx')
    plot(UEcglocx(i),UEcglocy(i),'rx')
end

%***cg location w/respect to hip***
cgloc=[UEcglocx,UEcglocy]-hip;

figure(2) %plot CoG angle
hold on
for i=1:length(cgloc)
    plot([0 cgloc(i,1)],[0 cgloc(i,2)])
end

%***Calculate UE Inertia***
%Ig=mk2
%J=Ig + mL2
Igforearm=m*FarmH*(forearml.*FarmHk).^2;
Iguarm=m*Uarm*(uarml.*Uarmk).^2;
Igthn=m*thn*(chestl.*thnk).^2;

Ig=2*Igforearm + 2*Iguarm +Igthn;
Ig=Ig';

%***calculate cog angle***
theta=atan2(cgloc(:,2),cgloc(:,1))-pi/2; %pi/2 means angle w/respect to vert.
%note L*sin(theta)=cgloc(:,1)
% L*cos(theta)=cgloc(:,2)

figure(3)
plot(theta*180/pi) %plot angle of cog

thetafilt=filtfilt(D,C,theta);

hold on
plot(thetafilt*180/pi,'r') %plot filter cog angle
theta=thetafilt;
title('cg angular displacement')

%***time derivatives of theta***
thetadot=ali_diff(thetafilt).*240; %cog angular vel.

figure(4)
plot(thetadot)
thetadot=FILTFILT(D, C, thetadot);
hold on
plot(thetadot,'-r')
title('cg angular vel')

```

```

figure(5)
hold on
thetaddot=ali_diff(thetadot).*240; %cog angular acc.
plot(thetaddot)
title('cg angular acc')

%****find chair acceleration****
%2 ways (but both arrive at exactly same curve)
%1
avgframe=(framec(:,1)+framef(:,1))/2000;
avgframev=ali_diff(avgframe)*240;

[B,A] = butter(2,12/120);
avgframevfilt=filtfilt(B,A,avgframev);

figure(6)
plot(-avgframev)
hold on
plot(-avgframevfilt,'r')
title('Wheelchair Velocity')

%2
%framecvx=-ali_diff(framec(:,1)).*240;
%framecvx=framecvx/1000;

%framefvx=-ali_diff(framef(:,1)).*240;
%framefvx=framefvx/1000;

%chairspeed=(framecvx+framefvx)/2;
%filtchair=filtfilt(B, A, chairspeed);
%plot(filtchair,'m')

%1 back to one
chairacc=ali_diff(avgframevfilt)*240; %PWC acceleration
chairaccfilt=filtfilt(B, A, chairacc);

figure(7)
plot(chairacc)
hold on
plot(chairaccfilt,'r')
title('Wheelchair Acceleration')
%plot(otheraccfilt,'g')

%****find end frame (chair input -> 0)****
accbackward=flipud(chairaccfilt);
lacc=length(chairaccfilt);
accbackward=accbackward(50:lacc-50,:);
index=min(find(abs(accbackward)>.05));
endx=lacc-50-index+3;
plot(endx,chairaccfilt(endx),'gx')
endx

%trim down to size
theta=theta(startx:endx,:);
thetadot=thetadot(startx:endx,:);

```

```

thetaddot=thetaddot(startx:endx,:);
chairaccfilt=chairaccfilt(startx:endx,:);
Ig=Ig(startx:endx);
%cgloc=cgloc(startx:endx,:);

%***dynamic model***
l=sqrt(cgloc(:,1).^2+cgloc(:,2).^2)./1000;
l=l(startx:endx,:);
phi=[thetadot theta];
r=phi'*phi;

xterm=UEm*chairaccfilt.*l.*cos(theta); %acc. term from PWC
nonlin=UEm*9.8067*1.*sin(theta); %gravity term of upper body
inertial=-UEm*(l.^2).*thetaddot; %inertial term from parallel axis
igterm=Ig.*thetaddot; %inertial term from parallel axi
%forcing=[-m*chairaccfilt.*cgloc(:,2) + m*9.8067*cgloc(:,1) -
m*l.^2.*thetaddot] - igterm;
forcing=[UEm*chairaccfilt.*l.*cos(theta) + UEm*9.8067*1.*sin(theta) -
UEm*l.^2.*thetaddot - igterm];

P=pinv(r)*(phi'*forcing); %pseudoinverse
P' %P' is 1x2 matrix containing B and K (damping, stiffness constants)

disp('program paused')
pause

%***Goodness of Fit***
X=P(1)*thetadot + P(2)*theta;
Y=forcing;

rho=corrcoef(X,Y);
rho=rho(1,2)

residual=(Y - X); %error in model
figure(18)
plot(residual)
figure(19) %error vs. cog angle
scatter(theta*180/pi,residual);
figure(20) %error vs. cog angular velocity
scatter(thetadot*180/pi,residual);

%***Calcualte a few PWC Parameters***

speed_at_brake=-avgframevfilt(startx);

speed_95=.95*speed_at_brake;
speed_05=.05*speed_at_brake;

startframe=min(find(-avgframevfilt<=speed_95));
endframe=min(find(-avgframevfilt<=speed_05));

figure(8) %shows on graph, velocity of PWC, start of brake
plot(-avgframevfilt); %and 95% & 5% of brake initiation speed
hold on

```

```

plot(startframe,-avgframevfilt(startframe),'xg')
plot(endframe,-avgframevfilt(endframe),'xr')

%***95/5 Braking Distance***
brake_dis=-((framec(endframe,1)-framec(startframe,1))+(framef(endframe,1)-
framef(startframe,1)))/2;
%brake_dis=-(framef(endframe,1)-framef(startframe,1));

%***95/5 Braking Time***
brake_time=(endframe-startframe)/240;

%***trunk angles***
[R,Col]=size(shoulder);

hiptoshould=[shoulder(:,1)-hip(:,1) shoulder(:,2)-hip(:,2)];
hiptoknee=[knee(:,1)-hip(:,1) knee(:,2)-hip(:,2)];
for i=1:R

trunkangle(i)=acos(dot(hiptoshould(i,:),hiptoknee(i,:))/(norm(hiptoshould(i,:
))*norm(hiptoknee(i,:)))));
end

figure(9)
trunkangle=trunkangle*180/pi;
plot(trunkangle)
trunkangle=filtfilt(D,C,trunkangle);
hold on
plot(trunkangle,'-r')
offset=trunkangle(startx);
trunkdisp=offset - trunkangle;
plot(trunkdisp,'-g')
title('trunk angular disp')

figure(10)
trunkvel=ali_diff(trunkdisp).*240; %trunk angular vel.
plot(trunkvel)
trunkvel=FILTFILT(D, C, trunkvel);
hold on
plot(trunkvel,'-r')
title('trunk angular vel')

figure(11)
trunkacc=ali_diff(trunkvel).*240; %trunk angular acc.
plot(trunkacc)
title('trunk angular acc')

maxtrunkdisp=max(trunkdisp);
maxtrunkvel=max(trunkvel);
maxtrunkdec=max(trunkacc);
max_acc=max(chairaccfilt);
%pause

cda_path
suggest=name;

[cda, cda_path] = uinputfile([suggest '.res'], 'Save As');

```

```

cd \
eval(['cd ' cda_path]);

fid=fopen(cda, 'w'); %open file for writing
fprintf(fid, '%f\t %f\t %f\t %f\t %f\t %f\t %f\t %f\t %f\t',
%f', P(1), P(2), speed_at_brake, maxtrunkdisp,
maxtrunkdec, brake_dis, brake_time, max_acc);
fclose(fid);

name=strtok(cda, '.');

lfile=[name '.l'];
resfile=[name '.err'];
igfile=[name '.ig'];

fid=fopen(lfile, 'w');
fprintf(fid, '%f\n', l);
fclose(fid);

fid=fopen(resfile, 'w');
fprintf(fid, '%f\n', residual);
fclose(fid);

fid=fopen(igfile, 'w');
fprintf(fid, '%f\n', Ig);
fclose(fid);

```

```

function [deriv]=ali_diff(thedata)

% Michael Dvorznak 8/14/97
% calculate derivative using:
% forward differencing (first term)
% 3-point central differencing (2 and last - 1)
% 5-point centered differencing (middle terms)
% backward differencing (last term)
% *****WARNING*****
% after ali_diff returns the derivative you
% need to divide by the sampling frequency

L=length(thedata);
for i=1:L,
    if i==1
        deriv(i)= (-thedata(i+2)+4*thedata(i+1)-3*thedata(i))/2;
    elseif i==2 | i==L-1
        deriv(i)= (thedata(i+1) - thedata(i-1))/2;
    elseif i==L
        deriv(i)= (3*thedata(i)-4*thedata(i-1)+thedata(i-2))/2;
    else
        deriv(i)= (-thedata(i+2)+8*thedata(i+1)-8*thedata(i-1)+thedata(i-
2))/12;
    end
end

deriv=deriv';

```

## BIBLIOGRAPHY

1. Cooper R, Dvorznak M, O'Connor T, Boninger M, and Jones D, Braking Electric-Powered Wheelchairs: Effect of Braking Method, Seatbelt, and Legrests, *Arch. Phys. Med. Rehabil.*, 79, 244-249, 1998.
2. Kirby RL, MacLeod DA, Wheelchair-Related Injuries Reported to the National Electronic Injury Surveillance System: an Update, *Proceedings of the 2001 Annual Conference*, 385-387, 2001.
3. Ummat S, Kirby RL, Nonfatal Wheelchair-Related Accidents Reported to the National Electronic Injury Surveillance System. *American Journal of Physical Medicine & Rehabilitation*, 73, 163-167, 1994.
4. Calder CJ & Kirby RL, Fatal Wheelchair-related Accidents in the United States, *American Journal of Physical Medicine and Rehabilitation*, 69(4), 184-190, 1990.
5. Viano DC, King AI, Melvin JW, Weber K, Injury Biomechanics Research: an Essential Element in the Prevention of Trauma. *Journal of Biomechanics*, 22(5), 403-417, 1989.
6. King AI & Yang K.H., Research in biomechanics of occupant protection. *The Journal of Trauma: Injury, Infection, and Critical Care*, 38(4), 570-576, 1995.
7. King AI, Viano DC, Mizeres N, States JD, Humanitarian Benefits of Cadaver Research on Injury Prevention, *The Journal of Trauma: Injury, Infection, and Critical Care*, 38(4), 564-569, 1995.
8. Foster J, Kortge J, Wolanin M, Hybrid III-A Biomechanically-Based Crash Test Dummy, *SAE Paper 770938*, 1977.
9. Society of Automotive Engineers, *Human Tolerance to Impact Conditions as Related to Motor Vehicle Design*. SAE Handbook Supplement HSJ885.
10. Kirby R, DiPersio M, MacLeod D, Wheelchair Safety: Effect of Locking or Grasping the Rear Wheels During a Rear Tip, *Arch. Phys. Med. Rehabil.*, 77, 1266-1270, 1996.
11. Sosner J, Fast A, Begeman P, Sheu R, and Kahan B, Forces, Moments, and Accelerations Acting on an Unrestrained Dummy During Simulations of Three Wheelchair Accidents, *Am. J. Phys. Med. Rehabil.*, 76, 304-310, 1997.

12. Fast A, Sosner J, Begeman P, Thomas M, and Durkman D, Forces, Moments, and Accelerations Acting on a Restrained Dummy During Simulation of Three Possible Accidents Involving a Wheelchair Negotiating a Curb, *Am. J. Phys. Med. Rehabil.*, 76, 370-377, 1997.
13. Tennant JA, Jensen RJ, & Potter RA, GM-ATD 502 Anthropomorphic Dummy – Development and Evaluation. *Proceedings of the Fifth International Technical Conference on Experimental Safety Vehicles*, London, England, 1974.
14. Kaleps I, Whitestone J, Hybrid III Geometrical and Inertial Properties, *SAE Paper 880638*, 1988.
15. Development of a flesh-like material, Fact sheet, Simula Government Products Inc., August 18, 1995.
16. VanIngen-Dunn C, Hurley TR, Yaniv G, Development of a Humanlike Flesh Material for Prosthetic Limbs, Simula Inc., 1995.
17. Dvorznak MJ, Cooper RA, O'Connor TJ, Boninger ML, Fitzgerald SG, Kinematic Comparison of Hybrid II Test Dummy to Wheelchair User, *Medical Engineering & Physics*, 23(4), 239-247, 2001.
18. OPTOTRAK: Measurement You Can Trust, NDI P/N 8300125, Jan. 2003.
19. Cooper RA, DiGiovine CP, Boninger ML, Shimada SD, Koontz AM, Baldwin MA, Filter Frequency selection for manual wheelchair biomechanics, *J. Rehabil. Res. Dev.*, 39(3), 323-336, 2002.
20. Winter DA, 'Biomechanics and Motor Control of Human Movement, Second Edition', John Wiley & Sons, Inc., New York, New York, 1990.
21. Duval-Beaupere G, Robain G, Upward Displacement of the Centre of Gravity in Paraplegic Patients, *Paraplegia*, 29, 309-317, 1991.
22. Shields RK, Muscular, skeletal, and neural adaptations following spinal cord injury. *J. Orthop. Sports Phys. Ther.*, 32, 65-74, 2002.
23. Kiratli BJ, Smith AE, Nauenberg T, Kallfelz CF, Perikash I, Bone mineral and geometric changes through the femur with immobilization due to spinal cord injury, *J. Rehabil. Res. Dev.*, 37, 225-233, 2000.
24. de Bruin ED, Herzog R, Rozendal RH, Michel D, Stussi E, Estimation of geometric properties of cortical bone in spinal cord injury, *Arch. Phys. Med. Rehabil.*, 81(2):150-156, 2000.

25. Lee TQ, Shapiro TA, Bell DM, Biomechanical properties of human tibias in long-term spinal cord injury. *J. Rehabil. Res. Dev.*, 34(3), 295-302, 1997.
26. de Bruin ED, Frey-Rindova P, Herzog RE, Dietz V, Dambacher MA, Stussi E, Changes of tibia bone properties after spinal cord injury: effects of early intervention, *Arch. Phys. Med. Rehabil.*, 80(2), 214-220, 1999.